CHALMERS
UNIVERSITY OF TECHNOLOGY

Application of isotherms models and error functions in activated carbon CO<inf>2</inf> sorption processes

Microporous and Mesoporous Materials 354 (2023) 112513

Contents lists available at ScienceDirect

Microporous and Mesoporous Materials

journal homepage: www.elsevier.com/locate/micromeso

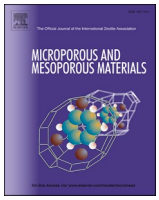

Application of isotherms models and error functions in activated carbon CO_2 sorption processes

Jarosław Serafin [a,*], Bartosz Dziejarski [b,c]

[a] Department of Inorganic and Organic Chemistry, University of Barcelona, Martí i Franquès, 1-11, 08028, Barcelona, Spain
[b] Faculty of Environmental Engineering, Wroclaw University of Science and Technology, 50-370, Wroclaw, Poland
[c] Department of Space, Earth and Environment, Division of Energy Technology, Chalmers University of Technology, SE-412 96 Gothenburg, Sweden

ARTICLE INFO

Keywords:
Isotherm data
Modeling
Error functions
Non-linear regression
CO_2 capture
Activated carbons

ABSTRACT

This work is concerned with the calculations using eight different isotherm models (Langmuir, Freundlich, Halsey, Temkin, Toth, Sips, Radke-Prausnitz, and Redlich-Peterson) to fit the experimental isotherm data of CO_2 on activated carbon (AC). Moreover, systematic and comprehensive modeling of non-linearized isotherms was performed by developing an algorithm for determining their parameters and analyzing seven error functions. To determine the best-fitted isotherm model and error function, we used the sum of normalized errors (SNE) procedure. The modeling results obtained showed that the Redlich-Peterson, Radke-Prausnitz, and Toth isotherm models are best suited to the empirical data, with relatively high R^2 determination coefficients. Finally, the SNE method allowed the selection of the chi-square test ($\chi 2$) and the HYBRID error as universal indicators in nonlinear regression to select the set of optimized isotherm parameters. The interpretation of the assumptions of the isotherm models, which featured a strong correlation with the experimental data, allowed a conclusion to be drawn about the sub-monolayer adsorption mechanism on the heterogeneous surface of the AC. The acquired modeling findings are expected to establish a certain theoretical foundation for the characterization of CO_2 adsorption equilibrium studies at the interface between porous solid materials and gases.

1. Introduction

The tremendous rise in CO_2 emissions into the atmosphere over several years is closely related to significant energy generation in the power industry. This sector directly uses the process of burning fossil fuels (mostly coal, crude oil, or natural gas processing products), whose reserves are rapidly depleting at an alarming rate due to their time of formation [1]. The world's demand for energy continues to soar due to a growing population and lifestyle changes, along with the most crucial environmental problem, such as climatic change, or more specifically, global warming [2]. In 2021, global CO_2 emissions increased by 6%, the highest level to date of 36.3 billion tonnes, according to the International Energy Agency (IEA). The analysis proved that this was a generic cause for the global economy to rebound from the COVID-19 pandemic crisis, using coal directly to stimulate its growth [3]. To find a solution to this worldwide issue, a great number of researchers have looked at extending the share of renewable energy sources (RES) and nuclear energy in the total balance of the energy system [4], the use of clean coal technologies (CCT) [5], and, above all, a wide spectrum of carbon capture, utilization, and storage technologies (CCUS) [6]. In light of the problems mentioned above, the adsorption process is swiftly becoming more well-known and is currently commonly used as a method of separation in CCUS systems with TRL of 2–5, along with other techniques such as absorption, membranes, cryogenic method, chemical looping combustion, or calcium looping. First, some of its benefits are as follows: high CO_2 capture efficiency (>85% vol. CO_2), large selection of materials, mild operating conditions, a wide range of operability, or low energy requirement [7]. The kind of adsorbent material that is used is the single most significantly essential factor in determining how effective the adsorption process is. Among them, carbonous materials have garnered a lot of attention owing to the rather unusual features they possess, especially activated carbons (AC). They are distinguished by being low in density, easy to modify in any way, developed pore structure, high surface area, chemical inertness and stability, low price and exhibit very high resilience to rapid changes in temperature and pressure [8]. As a result, AC is unquestionably the carbon-based material that has been subjected to the most in-depth study, which makes it not only incredibly effective but also extremely appealing for the purpose of

* Corresponding author.
E-mail address: jaroslaw.serafin@qi.ub.es (J. Serafin).

https://doi.org/10.1016/j.micromeso.2023.112513
Received 25 January 2023; Accepted 24 February 2023
Available online 1 March 2023

CO_2 capture.

Adsorption isotherms, which indicate the state of equilibrium as a function of the pressure of the adsorbate, may be used to specify how effective they are at capturing carbon dioxide. On top of that, in the process of characterizing porous materials, gas adsorption/desorption isotherm analysis is a technique that is used extensively, including parameters such as porosity, surface area, pore size, and pore size distribution. Therefore, the utilization of mathematical models for their description (fitting the obtained experimental data to the appropriate model of the adsorption isotherm) seems to be a reliable way to predict the behavior of activated carbons (AC) under a wide variety of process conditions. This step is vital for the efficient design of the adsorbate-adsorbent complex, as well as the scaling and optimization of the adsorption technology in the sense of the practical application of CO_2 uptake. Furthermore, equilibrium data at constant temperature provide key information on the nature and type of interaction between CO_2 and the surface of AC, also including a complete mechanism (development of the porosity of the solid, pore size distribution, chemical properties of the surface of AC, or values of thermodynamic parameters, enthalpy, Gibbs free energy, and standard entropy) [9]. In addition, comprehensive knowledge of the adsorption at the molecular level requires the identification of the equilibrium parameters using either a theoretical equation or an empirical value. Actually, in sorption studies, many two-parameter and three-parameter models are used. Langmuir, Freundlich, Hill, Temkin, Dubinin-Radushkevich, or Redlich-Peterson are just some examples. The equations most often used by scientists to determine adsorption isotherms are based primarily on the Langmuir and Freundlich model [10–12]. The selection of the relevant isotherm model (linear, or non-linear) compelling in evaluating one or more statistical criteria, defining the degree to which it correlates with the experimental data. The coefficient of determination (R^2), the sum of square errors (ERRSQ/SSE), the sum of absolute errors (SAE), the hybrid fractional error function (HYBRID), the percent standard deviation of Marquardt (MPSD), the average relative error (ARE), the chi-square test ($\chi 2$), are some of the error functions used to model the CO_2 adsorption process.

To date, a great deal of research by scientists has focused on modeling sorption isotherms for removing pollutants, including: foods (moisture reduction level) [13,14]; heavy metals [15,16], dyes [17,18] from aqueous media or volatile organic chemical mixtures [19,20]. In the case of mathematical modeling studies of adsorption equilibrium data concerning the removal of greenhouse gases from the mixture of fossil fuels, in particular CO_2, there are noticeable shortcomings in the well-description of this comprehensive procedure in the literature. Furthermore, there are a significant number of unanswered problems about the phase and sorption behaviors of CO_2 in increasingly complicated pore structures of different types of AC with heterogeneous surfaces and differing pore size configurations. This affects their levels of effectiveness for CO_2 adsorption, depending on their properties. Each type of AC raw material has its own unique features and optimal thermochemical conversion parameters. Precursors used to synthesize AC, such as biomass (andiroba shells [21], walnut shells [22], or garlic peels [23]) and industrial waste (surgical masks [24], fly ashes [25], or waste tiers [26]) influence the final characteristic of activated carbon related to the application of CO_2 capture. Hence, it is important to carefully consider the feedstock, thermochemical conversion parameters (temperature, activation time, residence time, heating rate), and especially guidance regarding CO_2 modeling equilibrium adsorption.

Therefore, in this paper, we aim to present the isotherm models and error functions that are most frequently selected, as a generic summary of a comprehensive modeling procedure for CO_2 adsorption on activated carbon (AC). Our work provides an important theoretical background and an in-depth understanding of the importance of CO_2 isotherm modeling. Consequently, this research can be considered as a basis for further improvement of low-TRL CO_2 capture systems with respect to the following: fundamental experimental methodology (advancing identification of promising materials for CO_2 sorption applications), design optimization (identifying the optimal operating conditions for a given adsorbent material), scaling up (distinguishing potential issues and opportunities related to the feasibility of the adsorption systems at larger scales), and commercialization (improving the performance and reducing the costs of the adsorption systems, making them more attractive for industry sector).

1.1. The theoretical foundations of adsorption isotherms modeling systems

To effectively remove CO_2 from the flue gas mixture, the synthesized sorbent material should have strictly defined desired properties and meet engineering and economic criteria [27]. First, they must be conducive to modeling the CO_2 adsorption system for design and optimization purposes. Moreover, their specific evaluation is obtained mainly based on the initial characteristics of the new materials and experimental studies on CO_2 adsorption isotherms - equilibrium data. The adsorbent, above all, must stand out by its high ability to effectively capture CO_2 from the flue gas under various process conditions and has a high potential for implementation in the industrial sector [28]. However, a single adsorbent rarely fulfills all these criteria. The current advantages of adsorption and the barriers that have to be overcome are illustrated in Fig. 1. At this time, there are a few key characteristics that pose the most important hurdles to the application of adsorption on an industrial level and an increase in technological maturity, which are: the manufacturing of adsorbents on a wide scale that is both cost-effective and efficient; a reduction in CO_2 uptake, as a result of the detrimental effects of contaminants in the flue gas mixture (water, SO_2, and NO); bringing the temperature of the flue gas down to the appropriate level by monitoring, controlling and regulation; and finally efficiently unite characterization studies with adsorption isotherms [29–32].

One of the essential issues for projecting and scaling up the adsorption process is the equilibrium adsorption capacity, which is directly related to the type of sorption and characterization of the material, including the specific surface, the pore size, and the surface chemistry of the sorbent. The value of the capacity indicates how many adsorbate molecules related to the adsorbent mass unit can be adsorbed at equilibrium (phase equilibrium at the solid-gas interface, where the adsorption rate is equal to the desorption rate). In terms of characterization and the characteristics of the pores (i.e. their size, shape, and morphology), the effectiveness of the sorbent is directly related to the micropores, as their size is comparable to the size of the gas molecules that can be adsorbed. Secondary roles are played by mesopores and macropores whose tasks are to transport the adsorbed gaseous medium through a network of channels, leading to active sites in micropores, located inside the solid body structure. Consequently, the step of evaluating the characterization of the perspective sorbent for use on an industrial scale is an important aspect of the verification procedure for the application of CO_2 adsorption [33–35].

The obtained experimental adsorption isotherm data is subsequently verified using mathematical models, which are now widely used in studies of the nature of the formed adsorption complex and in a detailed analysis of the mechanisms prevailing on the adsorbent surface. This procedure allows for a more realistic picture of the actual course of carbon dioxide adsorption while determining the factors affecting it, that is, course of the mechanism, temperature, CO_2 concentration/partial pressure in the gas mixture to be separated, the thermodynamic nature of the process, and detailed information on the theoretical evaluation and the use of the adsorbent in the form of a specific bed (specific surface area and its chemical properties, porosity and pore volume). Due to the correct interpretation of the parameters of the models used, it is possible to optimize the efficiency of CO_2 capture by the adsorbent. Ultimately, a techno-economic analysis is performed that highlights its potential for scaling and its application in many industries [36].

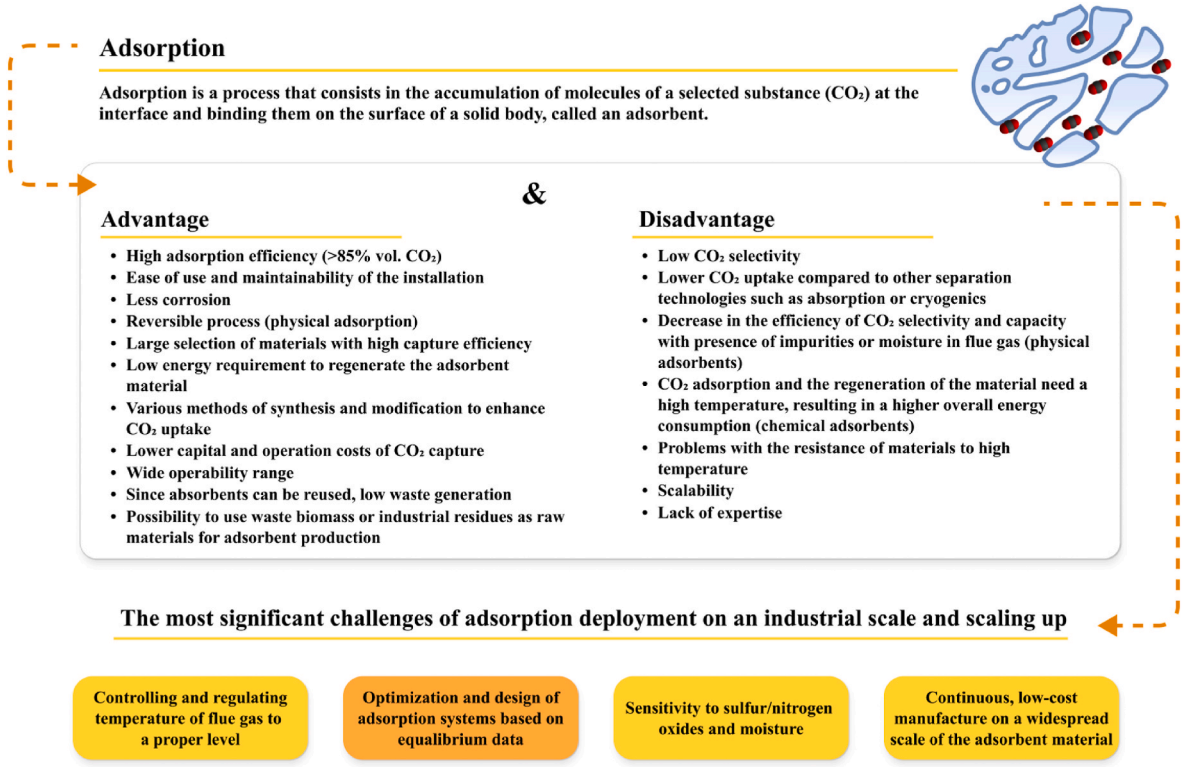

Fig. 1. State of the art of adsorption process and its upcoming challenges for increasing the technology readiness level (TRL).

1.2. The main types of sorption process

There are two main types of gas molecule adsorption on the surface of a solid. If the accumulation of the adsorbate on the surface of the solid occurs due to weak intermolecular van der Waals interactions, then adsorption is termed physisorption or physical adsorption [37,38]. When gas molecules accumulate on the surface of the adsorbent by chemical bonds, the phenomenon occurring is called chemical adsorption or chemisorption [39,40]. Both types are schematically shown in Fig. 2.

Chemical adsorption, also known as irreversible adsorption, is the process that is archived by substantial exchanging, or sharing, of electrons of adsorbate molecules with the adsorbent surface. The final result is the formation of a covalent or ionic bond [33]. Chemisorption is characterized by high interaction potentials, which lead to soar adsorption heat temperatures, often close to the value of chemical bonds

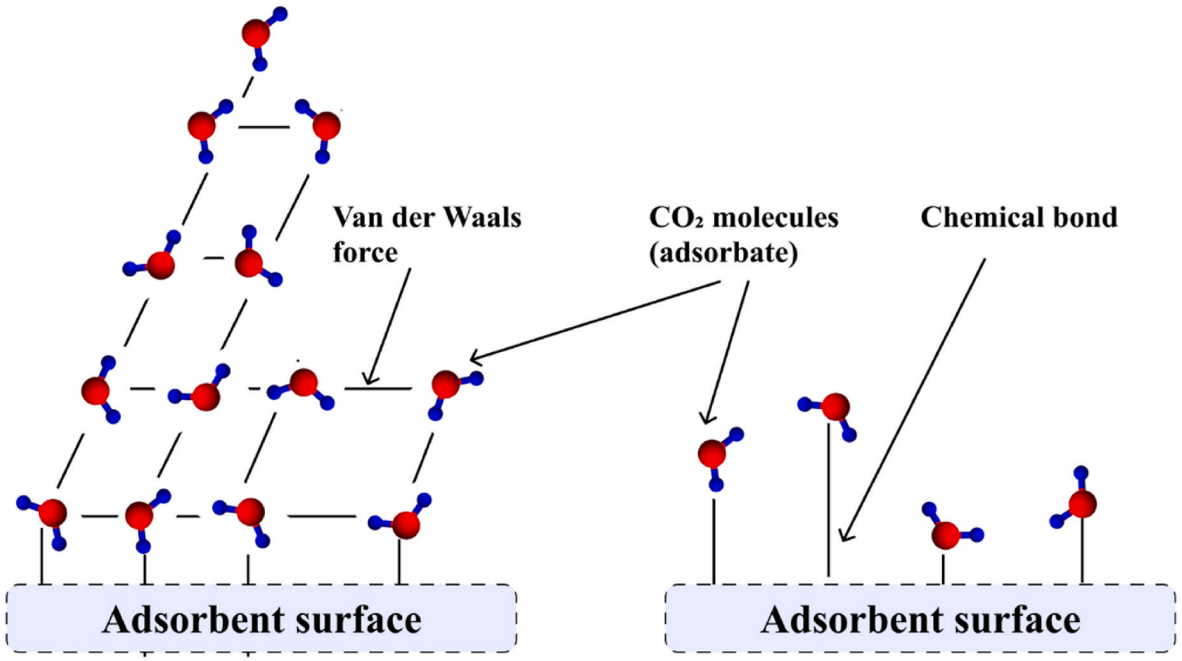

Fig. 2. The mechanism of physical (left) and chemical adsorption (right).

Table 1
Comparison of the physical and chemical adsorption mechanism [43].

Characteristic	Physisorption	Chemisorption
Type of bonding forces	The weak forces of Van der Waals	High forces, similar to a chemical bond
The thermal effect of the phenomenon	Low heat of adsorption, usually <40 kJ/mol	Large heat of chemisorption, 80–240 kJ/mol, up to the magnitude of the heat of chemical reactions
Equilibrium of adsorption and desorption	Complete reversibility	Partial irreversibility
Chemical change of adsorptive	None	Formation of a surface compound
The energy needed to establish an equilibrium	Very low (close to zero)	High activation energy needed
Course of the phenomenon	It is unbraked even at low temperatures, therefore fast	Only at higher temperatures is it no longer strongly braked
Specificity of adsorbate adsorbent interaction	No outstanding specificity	Outstanding specificity
Covering the surface with a solid as an adsorbent	Possible formation of multimolecular adsorption layers	Establishing the phenomenon with complete monomolecular coverage

(80–240 kJ/mol) [41]. As is also the case with most chemical reactions, it is often connected with a specific amount of activation energy, which is required to bring the system back to a state of equilibrium. Another critical aspect that affects the monolayer created is the arrangement of the molecules adsorbed on the surface. The adsorbate cannot move easily on the surface due to the establishment of chemical bonds between molecules and a specific site on the adsorbent. In the process of physical adsorption, van der Waals interactions occur between the adsorbate and the adsorbent, which are directed perpendicular to the boundary surface (as a result of dispersion forces or dipole interactions) [31]. Van der Waals forces are weak but long-range forces and have low enthalpy values (2040 kJ/mol). Due to them, a multilayer complex of adsorbate molecules can be formed on the surface of a solid [42].

The efficiency of the process in both types is closely related to the pressure and temperature; however, the characteristic features of each of them should be specified, due to a different mechanism, described in Table 1.

1.3. Classification of pores in adsorbent materials

The pore size of the porous adsorbent is commonly used to assess its adsorption capacity. The pore enables gas molecules to migrate from the solid's surface to its volume, where they are adsorbed. Aside from that, the adsorbent surface may be categorized into two types due to the pores: internal - defined as the area around closed pores, as well as the area surrounding all fissures and cracks that are deeper than their width, and external - defined primarily as superficial cracks of significant width [44]. The total surface of porous materials consists mainly of the inner surface; therefore, a greater amount of adsorption will be adsorbed in small pores, with a quite large depth in its structure.

Another critical topic is material porosity, which refers to the pores and their distribution collectively. Adsorption occurs exclusively in open pores, and hence the ratio of empty spaces and open pores to the volume occupied by the adsorbent is specified. Following the recommendations of the International Union of Pure and Applied Chemistry (IUPAC), pores can be divided into specific classes, which are given in Table 2 and Table 3 [45]. The classification of the main types of pores is presented in Fig. 3.

The size of the pores is an important aspect of the adsorption of gases in porous materials. Larger pores increase the amount of gas that can be adsorbed in the material and enhance the adsorption kinetics, but their size causes problems with the stability and structural penetration of the adsorbate. If the diameter of the pores is not large enough, the diffusion of adsorbates will be limited. It is more desirable for the adsorbent to have more small pores that increase the efficiency of the process through favorable interactions [46].

Table 2
Pore classification by the IUPAC according to the size [39].

Classification of pores	Diameter
Submicropores	<0.4 nm
Ultramicropores	<0.7 nm
Supermicropores	0.7–2 nm
Micropores	≤2 nm
Mesopores	2–50 nm
Macropores	>50 nm

Table 3
Pore classification by the IUPAC according to accessibility [39].

Classification of pores	Accessibility to surroundings
Open pore	Communicating with the external surface
Closed pore	No communicating with surroundings
Blind pore	Open only at one end
Through pore	Open at two ends

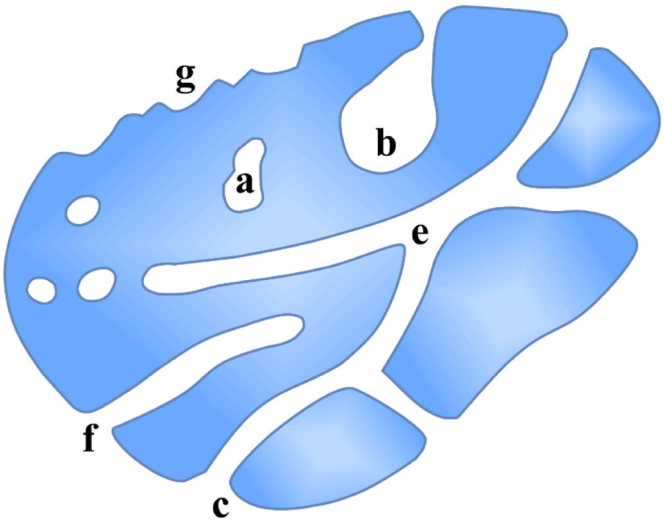

Fig. 3. Schematic classification of pores according to the IUPAC classification by accessibility to surroundings (a-closed pores; b, f-blind pores; c, d-open pores; e-through pores; g-roughness).

1.4. Mechanism of CO_2 adsorption at the solid-gas interface

The surface phenomenon known as adsorption may occur under any conditions, including pressure and temperature, if the CO_2 molecules and adsorbent are in intimate contact. The primary control factors are then either the adsorbate concentration or the partial pressure, depending on which one is being considered. As a consequence of the presence of strong interatomic and intermolecular forces [47], adhesion takes place at the contact boundary between two phases, more specifically at the interface between the solid and the gas [48]. Throughout the duration of the adsorption, the concentration of the gas agent varies, and the solid body has a tendency to attract and accumulate the adsorbate on its own surface. The mechanism of adsorption is strictly related to the resulting disproportion between the energy of the adsorbent surface (the inherited forces attract the molecules of gas) and molecules within its structure, where the forces are mutually balanced.

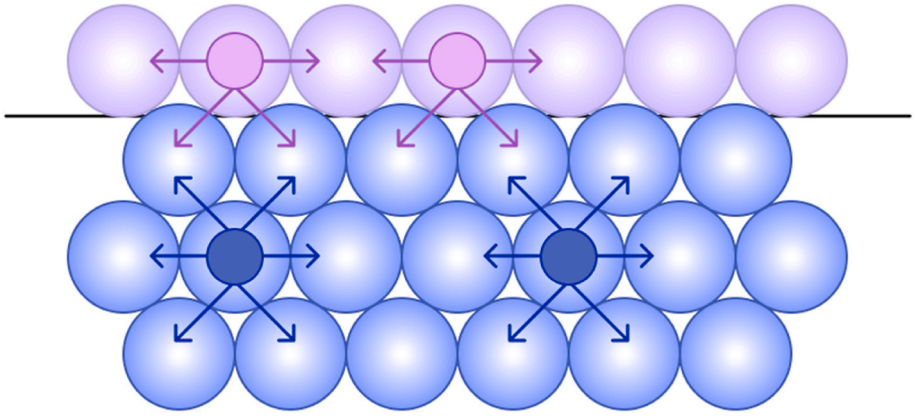

Fig. 4. Surface layer at the solid-gas interface.

That difference of forces is created by reactivity [49]. Fig. 4 shows a schematic representation of the forces at the solid-gas interface.

Adsorption is also a mass transfer process, when gas molecules come into contact with the adsorbent surface, the adsorption equilibrium is established after some specific time. This means that in the same unit of time, the same number of gas molecules is adsorbed as the number that is removed from the adsorbent surface (desorption) [50]. The amount of adsorbed adsorbate molecules per unit mass of adsorbent (m) is a function of the equilibrium pressure of the gas medium (p) and the process temperature (T), which can be formulated as follows:

$$m = f(p, T) \tag{1}$$

There are three parameters in this common equation; therefore, the adsorption equilibrium can be represented in the form of three equations, respectively, named the isotherm equation, adsorption isobar equation, and isosteres equation. The equilibrium data at constant temperature are used to a large extent in empirical research, because of their convenience, with the aim of developing the adsorption process in the industrial gas separation market [51–54]. Hence, adsorption isotherm models allow for a detailed analysis and estimation of the experimental findings under a variety of operating conditions to understand the nature of the adsorbent-adsorbate complex, which translates directly into optimization and increasing the TRL of adsorption technology in the industry. Along with studying the characteristics of potential materials for use in adsorption, they provide a rigorous method for verifying their ability to store CO_2.

2. Computational details

Numerous isotherm models and different approaches have been created for mathematical modeling over the years. One of the most useful methods for identifying the most accurate correlation, measuring the distribution of the adsorbate, and enabling the theoretical analysis of the adsorbate-adsorbent complex is linear regression, which has been used extensively. It is closely related to aspects of the straightforward nature of the linear equation and the versatility with which it may be used in a broad variety of ranges of process parameters, such as temperature or pressure. However, over time, it has been established that the non-linear regression methodology is the most effective way to choose the best-fitted isotherm [55–59]. It enables us to skip the transformation of isotherm non-linear equations into their linearized forms and eliminate any inherent bias that may have an influence on an incorrect interpretation of the isotherm model parameters along with making inappropriate use of them the gain insight into the design of adsorption systems [60]. Moreover, non-linear regression comprises the precise procedure of reducing the error distribution between the experimental equilibrium data and the curve of predicted ones from the anticipated isotherm model [61]. Finally, to assess the fit of a certain isothermal curve, this optimization process requires the specification of error functions, which will be discussed deeply in the next section.

Considering the above, we employed eight widely reported adsorption isotherm models in this study to model the CO_2 adsorption equilibrium data on activated carbon (AC), including two-parameters (Langmuir, Freundlich, Halsey, and Temkin), and three-parameters (Toth, Sips, Redlich-Peterson, and Radke-Prausnitz). To detailed estimate the parameters of the selected isotherms, the nonlinear optimization technique was implemented, utilizing Excel's Solver Add-in with Origin's NLfit tool to perform the verification and validation of the concluding results. The non-linear equations of examined isotherm models, together with their respective theoretical assumptions and a detailed explanation of the parameters, are provided and explained in more complexity below.

2.1. Theoretical outlook on the modeling of the adsorption equilibrium systems

2.1.1. Two-parameters isotherm models

2.1.1.1. Langmuir isotherm model. The Langmuir isotherm is applied to monolayer adsorption occurring at homogeneous sites on the surface of solid adsorbent material. The model assumes that there are a certain number of active sites on the surface of a solid, each of which can adsorb only one adsorbate molecule. The achievement of an equilibrium state should be interpreted as the occupation of all active centers on the surface by adsorbed molecules and the formation of a monomolecular layer. In other words, the Langmuir isotherm is characterized by a monotonic approach to boundary adsorption, which corresponds to the monomolecular adsorption layer covering the entire surface of the solid body [62,63]. Moreover, it is assumed that between the molecules adsorbed on the surface of the adsorbent there is no interaction, and the heat of adsorption is constant and independent of the degree of surface coverage [64,65]. The nonlinear equation of the Langmuir isotherm model takes the following form:

$$q_e = q_m \frac{K_L \cdot P}{(1 + K_L \bullet P)} \tag{2}$$

where, P is relative pressure of the adsorbate [Pa], q_e is the amount of adsorbed adsorbate at equilibrium state (mol/g), q_m is maximum monolayer adsorption capacity (mol/g), and K_L is equilibrium constant between the gas and adsorbed phases (1/Pa).

2.1.1.2. Freundlich isotherm model. The Freundlich isotherm model is a purely empirical equation with no theoretical basis and is not limited to the formation of a monolayer. It describes the non-ideal, reversible process of monolayer or multilayer adsorption on a heterogeneous

surface [66]. In Freundlich's theory, the number of adsorbed molecules with complete coverage of the adsorbent surface cannot exceed the number of active sites. Moreover, unlike the Langmuir model, which states that the heat of adsorption does not change with the surface coverage of the adsorbent, Freundlich's model is based on the assumption that the adsorption energy logarithmically decreases as the number of available adsorption sites decreases (with increasing coverage of the adsorbate on the surface of the solid) [67]. The equation of the Freundlich model in nonlinear form takes the following mathematical representation:

$$q_e = K_F \cdot^{P^{n_F}} \tag{3}$$

where, K_F is Freundlich constant (1/Pa), and n_F is heterogeneity factor (−). Physisorption is indicated when the value of n_F is more than one, whereas chemisorption is shown by a number that is less than unity [68].

2.1.1.3. Temkin isotherm model. The Temkin isotherm model is an experimental two-parameter equation of adsorption isotherm on a heterogeneous solid, which assumes that the adsorption process is characterized by a uniform, infinite (unlimited minimum or maximum energy) energy distribution of the adsorption sites on the adsorbent surface [69]. The Temkin model disregards both the very high and extremely low amounts of concentration of adsorbate. It also takes into account the influence of indirect interactions between the adsorbate and the adsorbent on the heat of adsorption of the adsorbed molecules in the layer, which decreases linearly rather than logarithmically (as in the case of Freundlich's model) with increasing solid surface coverage [70,71]. As a result of these assumptions, adsorption is characterized by a continuous distribution of the bond energy in the adsorption complexes. The equation of the Temkin model in a non-linearized form takes the form:

$$q_e = B \bullet \ln(K_T \cdot P) \tag{4}$$

where, B is Temkin constant (−), and K_T is adsorption equilibrium constant (1/Pa).

The Temkin constant can be formulated as follows:

$B = \frac{R \cdot T}{b}$ where, R is universal gas constant (J/mol·K), T is temperature (K), and b is parameter related to the adsorption energy (J/mol).

Parameter b of the model can be written as:

$$b = \Delta Q = -\Delta H_{ads} \tag{6}$$

where: ΔQ is change in adsorption energy (J/mol), ΔH is change in heat of adsorption (J/mol). If the value of parameter b is positive, it means that the adsorption process is exothermic. On the other hand, the negative value of parameter b determines the endothermic nature of adsorption.

2.1.1.4. Halsey isotherm model. The Halsey isotherm model is applicable for multilayer adsorption systems that include heterogeneous surfaces of adsorbents, in which the heat from adsorption is not evenly distributed [72]. It also assumes that condensation of adsorption occurs at a comparatively great distance from the surface. The Halsey model equation in non-linearized form is presented as follows:

$$q_e = e^{\frac{[\ln(K_H) - \ln(P)]}{n_H}} \tag{7}$$

2.1.2. Three-parameters isotherm models

2.1.2.1. Toth isotherm model. The Toth isotherm model is an additional helpful modification of the Langmuir model, which increases the accuracy of the predicted value to the experimental findings, by taking into account the presence of submonolayer coverage [73–75]. It is applied to describe adsorption occurring on heterogeneous surfaces with a wide variety of absorbate concentrations, both low and high [58]. The Toth model also assumes an asymmetrical Quasi-Gaussian energy distribution extended toward low adsorption energies [76]. The expression for the nonlinear Toth isotherm model may be found down below:

$$q_e = \frac{q_m \cdot K_T \cdot P}{[1 + (K_T \cdot P)^{n_T}]^{\frac{1}{n_T}}} \tag{8}$$

where, q_m - maximum adsorption capacity (mmol/g), K_T - Toth isotherm constant (bar^{-1}), n_T - heterogeneity factor (−). If the surface is homogenous, then n_T equals one, there is no difference in the relative energies of the various adsorption sites, and the Toth equation is reduced to the Langmuir equation.

2.1.2.2. Sips isotherm model (Langmuir-Freundlich). The Sips isotherm model is a combined form of the Langmuir and Freundlich model equations [77]. It was developed for the purpose of forecasting the heterogeneous adsorption systems and eliminating the constraint imposed by the growing concentration of adsorbate that is experienced when using the Freundlich isotherm model. As a result, at a low concentration of adsorbate, this model becomes equivalent to the Freundlich isotherm, while it predicts monolayer adsorption at high concentrations, which is indicative of the Langmuir isotherm [78,79]. The nonlinear Sips isotherm may be quantitatively expressed by the following equation:

$$q_e = \frac{q_m \cdot (K_S \cdot P)^{\frac{1}{n_S}}}{1 + (K_S \cdot P)^{\frac{1}{n_S}}} \tag{9}$$

where, q_m is maximum adsorption capacity (mmol/g), K_s is Sips isotherm constant (bar^{-1}), and n_s is Sips isotherm exponent (−).

2.1.2.3. Redlich-Peterson isotherm model. Integrating the Freundlich and Langmuir isotherms leads to the formation of the Redlich–Peterson model, which consists of three different parameters [80]. This empirical isotherm model is used to accurately portray adsorption equilibrium conditions over a broad concentration range of adsorbate that can be employed in either homogenous or heterogenous systems, due to its adaptability [81,82]. At large concentrations of adsorbate, Redlich-Peterson isotherm reduces to the Freundlich model, and the exponent β_{RP} tends toward zero. However, for low concentrations, it reduces to the Langmuir model, owing to the fact that the β_{RP} value approaches one [83]. The nonlinear form of the Redlich-Peterson isotherm model is represented by the following equation:

$$q_e = \frac{K_{RP} \cdot P}{1 + a_{RP} \cdot P^{\beta_{RP}}} \tag{10}$$

where, K_{RP} is Redlich-Peterson isotherm constant (bar^{-1}), a_{RP} is a constant (bar^{-1}), and β_{RP} is the exponent, which may range from 0 to 1 in value (−).

2.1.2.4. Radke-Prausnitz isotherm model. The Radke-Prausnitz isotherm model is typically applied in adsorption systems when the concentration of the adsorbate is relatively low [84]. The following expression provides a mathematical representation of the Radke-Prausnitz isotherm model:

$$q_e = \frac{q_m \cdot K_{RPr} \cdot P}{1 + K_{RPr} \cdot P^{e_{RPr}}} \tag{11}$$

where, q_m is maximum adsorption capacity (mmol/g), K_{RPr} is Redlich-Prausnitz isotherm constant (bar^{-1}), and e_{RPr} is the model exponent (−).

2.2. Error functions, as an isotherm model fitting selection criterion

To assess the fit of adsorption isotherm models for the analysis and

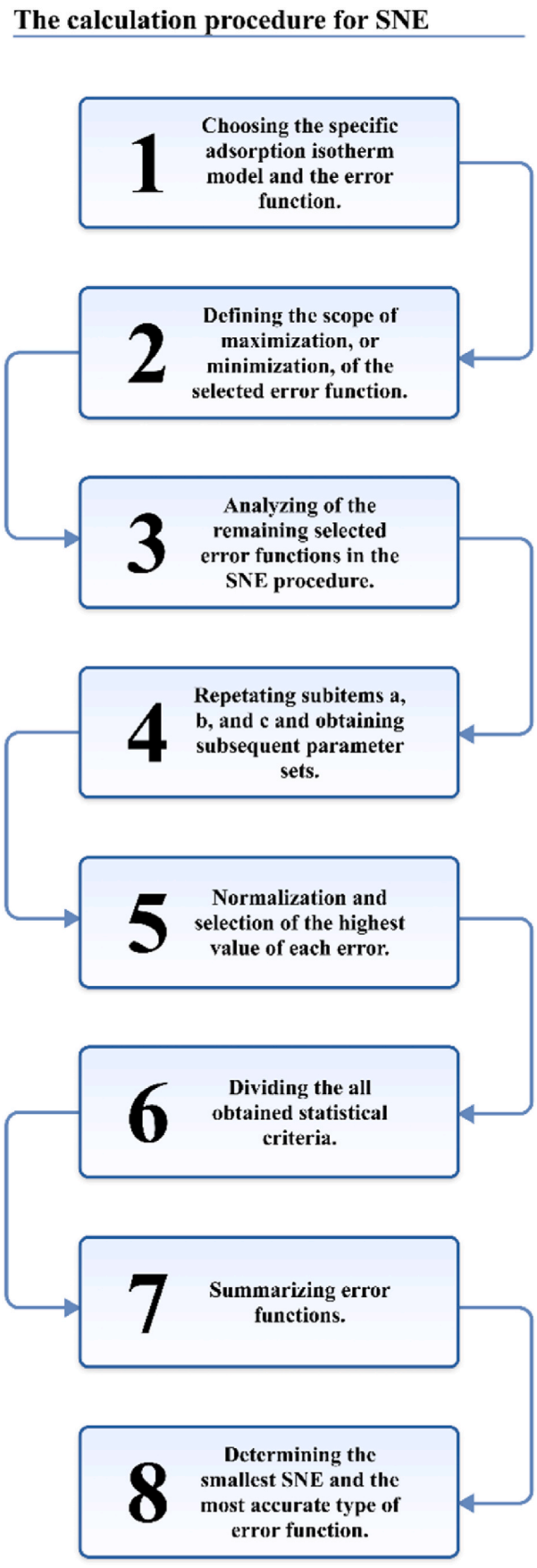

Fig. 5. SNE process determination for selection of the optimum error function and set of isotherm parameter, best correlating with the experimental data.

design of a specific adsorption system, statistical criteria, known as error functions, are significantly required. Evaluation of the accuracy of the isothermal model curves in relation to the experimental data enables verification of the theoretical assumptions of the adsorbate-adsorbate interactions on a solid porous material. Consequently, the error functions allow to estimate the differences between the predicted and experimental amounts of adsorbed CO_2 at the equilibrium state. The ultimate selection of an isotherm is defined by a comparison of one or more of them, indicating the magnitude of compliance with the requirements regarding best-fitting. In this study, we examined seven error functions, which are: coefficient of determination (R^2), sum of squares error (ERRSQ/SSE), average relative error (ARE), the hybrid fractional error function (HYBRID), Marquardt's percent standard deviation (MPSD), the sum of absolute errors (SAE), and chi-square test (χ^2), by minimizing the respective error function across the relative pressure of adsorbate. In the section that follows, error functions are examined in great depth.

Since each error function is likely to provide a different set of isotherm parameters and affect them directly in the sense of the accuracy of fitting, there are many difficulties in identifying the optimum ones. It is important to note that there is no single one that is considered the best for all sorption systems and that the choice of the criterion depends on the specific characteristics of the adsorbent and adsorbate, as well as the range of the experimental data. Therefore, it is recommended to use multiple methods for model selection and comparison. In view of this, we applied a conventional procedure to normalize and combine the value of all the error functions used in the adsorption equilibrium modeling for a better and meaningful comparison between the set of model parameters, called the sum of normalized errors (SNE) [85,86]. Using SNE, the set of isotherm parameters that provides the best fit to the experimental data is identified by comparing the scaled errors directly [87]. The minimum SNE value is considered as a final indicator for choosing the optimal type of error function and on its basis, the best-fitted set of parameters for the examined single isotherm model. The sum of the normalized error calculation procedure is presented in Fig. 5. The following is the methodology that is utilized to evaluate the SNE:

a) Choosing the specific adsorption isotherm model and the error function for non-linear regression to determine the parameter set of the model equation.
b) Define the scope of maximization, or minimization, of the selected error function (for R^2 it is defined by 1, while for the rest of the errors it is 0).
c) Analysis of the remaining selected error functions in the SNE procedure that are calculated from the obtained predicted isotherm model data in the same parameter set.
d) Repetition of subitems a, b, and c and obtaining subsequent parameter sets of the same isotherm model related to the specific error function.
e) Normalization and selection of the highest value of each error derived from all the parameter sets.
f) Dividing all obtained statistical criteria by their highest value in the entire normalization procedure.
g) Summation of error functions from specific parameters sets to obtain SNE values related.
h) Determination of the smallest SNE and the most accurate type of error function, which provides the best fit of the isotherm model curve to the experimental data.

2.2.1. *The coefficient of determination (R^2)*

The quality of the fit of isothermal models to the experimental data is usually assessed based on the value of the coefficient of determination [88], which represents the variance of the mean value [89]. The closer the value of R^2 is to one, the better the fit of the tested model is ensured.

The coefficient of determination is expressed as follows [90]:

$$R^2 = \frac{\sum_{i=1}^{n}\left(q_{e,mod} - \overline{q_{e,exp}}\right)^2}{\sum_{i=1}^{n}\left(q_{e,mod} - \overline{q_{e,exp}}\right)^2 + \sum_{i=1}^{n}\left(q_{e,mod} - q_{e,exp}\right)^2} \quad (12)$$

2.2.2. The sum of the squares error (ERRSQ/SSE)

The sum of squares errors (ERRSQ/SSE) is the most widely reported error function in isotherm modeling [55]. However, the major disadvantage of ERRSQ/SSE is that at higher relative pressure, the error squares increase. This results in a better fit, which does not always reflect the true nature of the adsorption complex. The sum of the squares error is defined as the equation [55]:

$$ERRSQ = \sum_{i=1}^{n}\left(q_{e,exp} - q_{e,mod}\right)^2 \quad (13)$$

2.2.3. The sum of absolute errors (SAE)

The sum of the absolute errors (SAE) is a similar error function to the sum of squared deviations (ERRSQ/SSE) [80]. In such a case, fitting the isotherm model to the measurement data using this error function would provide a better fit at higher relative pressure. The SAE is presented by the formula [91]:

$$EABS = \sum_{i=1}^{n}\left|q_{e,\exp} - q_{e,mod}\right| \quad (14)$$

2.2.4. The hybrid fractional error function (HYBRID)

The hybrid fractional error function (HYBRID) was developed to improve the fit of the sum of squares error (ERRSQ/SSE) at low relative pressure by dividing it by the measured experimental value [92]. Furthermore, the equation considers he number of degrees of freedom (the difference between the number of measurement points (N) and the number of variable parameters (p)). The HYBRID error is defined as [93]:

$$HYBRID = \frac{100}{N-p}\sum_{i=1}^{n}\left[\frac{\left(q_{e,\exp} - q_{e,mod}\right)^2}{q_{e,\exp}}\right] \quad (15)$$

2.2.5. The Marquardt's percent standard deviation (MPSD)

The percentage standard deviation according to Marquardt is related to the geometric mean of the error distribution modified according to the number of degrees of freedom in the isotherm model [94]. The MPSD error is determined by the following equation [95]:

$$MPSD = 100\sqrt{\frac{1}{N-p}\sum_{i=1}^{n}\left(\frac{q_{e,\exp} - q_{e,mod}}{q_{e,\exp}}\right)^2} \quad (16)$$

2.2.6. The average relative error (ARE)

The average relative error (ARE) was created by Marquardt with the intention of minimize the distribution of the fractional error over the entire range of relative pressure (independent variables) [96]. The ARE error is expressed as follows [97]:

$$ARE = \frac{100}{N}\sum_{i=1}^{n}\left|\frac{q_{e,\exp} - q_{e,mod}}{q_{e,\exp}}\right| \quad (17)$$

2.2.7. The chi-square test (χ^2)

The chi-square test is a very important error function in determining the best fit of the isotherm model to the tested adsorption system. It is possible to estimate it by finding the difference in squares between the model data that was predicted and the data that was actually collected, then dividing each difference by the corresponding experimental value. The error χ^2 is defined by the following equation [84]:

$$\chi^2 = \sum_{i=1}^{n}\frac{\left(q_{e,mod} - q_{e,\exp}\right)^2}{q_{e,\exp}} \quad (18)$$

Where: $q_{e,mod}$ - predicted amount of adsorbed adsorbate at equilibrium state [mmol/g], $q_{e,exp}$ - experimental amount of adsorbed adsorbate at equilibrium state [mmol/g], $\overline{q_{e,exp}}$- mean value of $q_{e,exp}$ [mmol/g], N - number of measurement points of experimental data [−], p – the number of variable parameters in the equation of the isotherm model.

3. Results and discussion

The data used in this work was taken from our earlier research on activated carbon from pomegranate peels, where we presented the entire physicochemical characteristics of the obtained series of activated carbon [98]. The experimental CO_2 adsorption equilibrium data on activated carbon (AC) from the pomegranate peels at two temperatures of 0, and 25 °C were evaluated using the non-linear curve fitting sum of normalized error (SNE) procedure. SNE was crucially adopted to directly determine the choice of the optimum error function, the parameter set, and ultimately the best-fitting isotherm model. Overall, this included minimizing the effects of a single error function while simultaneously computing the other error values that have been comprehensively investigated in this study. Of all AC samples that have been activated at four different temperatures (600, 700, 800, and 900 °C), AC-800 has shown the highest CO_2 adsorption capacity of 5.53, 4.44 mmol/g for 0 and 25 °C at atmospheric pressure, respectively. Hence, we chose it as a representative example in the error function analysis of the adsorption isotherms. Additionally, with reference to the article [92], it has been proven that AC-800 sample likely achieved the best CO_2 uptake due to its structural and textural characteristics, specifically the largest BET surface area, total pore volume and micropore volume. Activation temperature directly affected CO_2 adsorption, as its mechanism is strongly influenced by the size and distribution of pores in the AC material. Accordingly, 800 °C has been determined to be the optimum temperature during activation, as it led to the formation of a large micropores. That simultaneously increased both the specific surface area and the number of available adsorption sites, providing an optimal environment for CO_2 capture among the activated samples at different temperatures. In summary, the development of porosity was examined as the most essential factor influencing the mechanism of CO_2

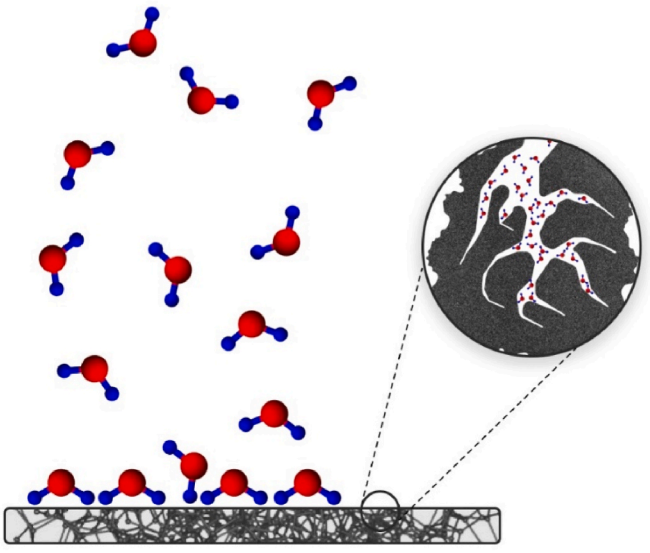

Fig. 6. Mechanism of CO_2 adsorption on investigated activated carbon samples.

Table 4
Summarization of the determined error functions, sum of normalized errors (SNE), and parameter sets of the non-linear Langmuir isotherm model for AC-800.

	R^2	ERRSQ/SSE	ARE	χ2	HYBRID	MPSD	EABS
Temperature 0 °C							
K_L	2.2535	2.2652	3.788	2.9519	2.9519	3.8149	2.3683
q_m	7.8128	7.7863	6.2707	6.9707	6.9707	6.1616	7.6085
R^2	0.997929	0.997926	0.988881	0.995891	0.995891	0.986874	0.997819
ERRSQ	0.359029	0.358513	1.736549	0.683417	0.683417	1.990773	0.372078
ARE	15.580369	15.496994	6.040002	9.439708	9.439708	6.090364	14.586652
χ2	0.517337	0.512165	0.513813	0.296384	0.296384	0.524590	0.458137
HYBRID	1.124646	1.113403	1.116985	0.644314	0.644314	1.140413	0.995949
MPSD	0.198586	0.197645	0.073926	0.115500	0.115500	0.072793	0.186198
EABS	3.732897	3.709755	5.557537	3.915185	3.915185	5.744248	3.631505
SNE	5.807925	5.773798	5.551652	**4.343543**	4.343543	5.748482	5.444510
Temperature 25 °C							
K_L	1.3090	1.3156	1.8363	1.5503	1.5503	1.8807	1.2995
q_m	7.8069	7.7819	6.4608	7.1282	7.1282	6.3993	7.8176
R^2	0.998551	0.999457	0.997696	0.997594	0.997594	0.992926	0.998529
ERRSQ	0.084542	0.084460	0.345253	0.135032	0.135032	0.370719	0.085570
ARE	6.321370	6.275618	4.089008	4.829069	4.829069	4.161500	6.427680
χ2	0.103697	0.102125	0.107751	0.069924	0.069924	0.117816	0.109057
HYBRID	0.414788	0.408501	0.431004	0.279697	0.279697	0.471265	0.436227
MPSD	0.099245	0.098476	0.051783	0.068146	0.068146	0.051125	0.101917
EABS	1.372133	1.370727	2.155000	1.606149	1.606149	2.271842	1.346719
SNE	5.549591	5.508306	5.852404	4.677202	**4.677202**	6.143438	5.674889

Table 5
Summarization of the determined error functions, sum of normalized errors (SNE), and parameter sets of the non-linear Freundlich isotherm model for AC-800.

	R^2	ERRSQ/SSE	ARE	χ2	HYBRID	MPSD	EABS
Temperature 0 °C							
K_F	5.91834	5.8961	6.9198	6.1976	6.1976	7.2273	6.0099
n_F	0.60839	0.6059	0.7366	0.6796	0.6796	0.7731	0.6245
R^2	0.995521	0.995504	0.972783	0.991401	0.991401	0.960951	0.995202
ERRSQ	0.723331	0.720591	6.062083	1.520939	1.520906	9.527079	0.798935
ARE	40.430735	41.245645	14.473847	18.754386	18.754604	16.398340	34.799100
χ2	1.858150	1.932588	1.485869	0.732455	0.732455	2.352835	1.396320
HYBRID	4.039456	4.201278	3.230150	1.592294	1.592294	5.114858	3.102932
MPSD	0.784976	0.800019	0.234417	0.380822	0.380826	0.199079	0.681525
EABS	5.307359	5.325995	9.556287	5.877570	5.877538	12.251787	5.244120
SNE	5.050053	5.153105	4.300430	**3.188568**	3.188573	5.611695	4.407272
Temperature 25 °C							
K_F	4.6777	4.6702	4.8985	4.7854	4.7854	5.0161	4.6986
n_F	0.6649	0.6631	0.7263	0.7053	0.7053	0.7504	0.6650
R^2	0.997588	0.999134	0.997520	0.996113	0.996113	0.989444	0.997524
ERRSQ	0.131718	0.131449	0.394490	0.226496	0.226496	0.691091	0.136491
ARE	9.210621	9.371613	5.664600	6.048124	6.048124	6.115476	9.291468
χ2	0.207856	0.215305	0.143990	0.120728	0.120728	0.220924	0.213949
HYBRID	0.831425	0.861221	0.575961	0.482912	0.482912	0.883698	0.855796
MPSD	0.182034	0.185481	0.085358	0.107652	0.107652	0.074957	0.184577
EABS	1.716645	1.714970	2.403854	1.972595	1.972595	3.115059	1.701096
SNE	5.586061	5.689876	4.709059	4.276654	**4.276654**	6.046978	5.665405

adsorption, especially large volume micropores in AC-800 - the narrow micropores (<0.8 nm), which allowed small CO_2 molecules (~0.33 nm) to easily penetrate within activated carbon structure along with efficient and selective sorption (Fig. 6).

Tables 1–8 depict the different parameter sets of all the studied non-linear isotherm models of CO_2 adsorption data for AC-800, as well as the analysis of error functions, which include the procedure of sum of normalized errors (SNE). The examination of the smallest SNE values for the particular isotherm model enables the specification of foremost isotherm parameter set that provides the most satisfactory approximation between the experimental and predicted data, along with identified the isotherm models fitting selection criteria. The rest of the modeling results for the AC-600, AC-700, and AC-900 samples are included in Tables S1–S16. The minimal values of SNE for an adequate error function are indicated by the numbers that are bolded and underlined, with regard to every individual isotherm model and every single sample of activated carbon (AC).

Evaluation and interpretation of the calculated values of the individual sum of normalized errors greatly facilitate the selection of the most convenient and precise optimization criteria among the seven error

Table 6
Summarization of the determined error functions, sum of normalized errors (SNE), and parameter sets of the non-linear Halsey isotherm model for AC-800.

	R^2	ERRSQ/SSE	ARE	$\chi 2$	HYBRID	MPSD	EABS
Temperature 0 °C							
K_H	0.0538	0.0535	0.0725	0.0683	0.0683	0.0774	0.0561
n_H	−1.6437	−1.6504	−1.3606	−1.4714	−1.4714	−1.2936	−1.6072
R^2	0.995521	0.995504	0.974207	0.991401	0.991401	0.960949	0.995258
ERRSQ	0.723331	0.720591	5.670653	1.520912	1.520913	9.527703	0.788162
ARE	40.430046	41.245353	14.471942	18.754784	18.754784	16.398332	35.641159
$\chi 2$	1.858087	1.932561	1.416232	0.732455	0.732455	2.352941	1.460675
HYBRID	4.039320	4.201219	3.078765	1.627678	1.592294	5.115089	3.175381
MPSD	0.784964	0.800013	0.236159	0.385038	0.380830	0.199079	0.697069
EABS	5.307339	5.325991	9.316241	5.877532	5.877532	12.252053	5.243265
SNE	5.049894	5.152993	4.184013	3.200717	**3.188540**	5.611697	4.487431
Temperature 25 °C							
K_H	0.0982	0.0979	0.1122	0.1086	0.1086	0.1166	0.0977
n_H	−1.5040	−1.5080	−1.3767	−1.4179	−1.4179	−1.3326	−1.5027
R^2	0.997588	0.999134	0.997510	0.996113	0.996113	0.989444	0.997510
ERRSQ	0.131718	0.131449	0.396149	0.226499	0.226488	0.691090	0.137520
ARE	9.210814	9.371403	5.664656	6.048105	6.048185	6.115465	9.255405
$\chi 2$	0.207865	0.215295	0.144262	0.120728	0.120728	0.220924	0.212536
HYBRID	0.831461	0.861180	0.577050	0.482912	0.482912	0.883695	0.850144
MPSD	0.182039	0.185476	0.085330	0.107651	0.107654	0.074957	0.183839
EABS	1.716638	1.714976	2.407169	1.972602	1.972574	3.115053	1.702432
SNE	5.586239	5.689792	4.714869	4.276689	**4.276686**	6.047002	5.646746

Table 7
Summarization of the determined error functions, sum of normalized errors (SNE), and parameter sets of the non-linear Temkin isotherm model for AC-800.

	R^2	ERRSQ/SSE	ARE	$\chi 2$	HYBRID	MPSD	EABS
Temperature 0 °C							
B	1.0037	0.8635	0.0985	0.2975	0.2975	0.0975	0.9181
K_T	118.8407	157.1366	1267.5418	656.0070	656.0070	1292.7293	122.3163
R^2	0.877444	0.860327	0.281125	0.273563	0.273563	0.281175	0.868956
ERRSQ	27.060423	23.280823	219.983791	108.876581	108.876580	220.585698	24.554522
ARE	1.155425	473.651652	52.121889	111.572702	111.572703	52.257402	565.892516
$\chi 2$	575.976086	325.993156	52.602664	33.927953	33.927953	52.766645	469.484263
HYBRID	1252.121927	708.680773	114.353618	73.756420	73.756420	114.710097	1020.617963
MPSD	23.500290	17.681812	0.616985	2.048019	2.048019	0.616709	21.235201
EABS	27.760167	27.848011	64.373373	47.365318	47.365318	64.486343	27.095331
SNE	4.555198	4.239251	2.616925	1.941975	**1.941975**	2.622261	5.055648
Temperature 25 °C							
B	1.1357	1.0369	0.4988	0.7414	0.7414	0.4645	1.1487
K_T	33.8360	40.5346	97.3483	71.6896	71.6899	107.8795	30.1430
R^2	0.919971	0.968196	0.796063	0.730480	0.730479	0.414679	0.916027
ERRSQ	5.345245	4.880264	31.177453	10.024311	10.024356	35.037866	5.791273
ARE	74.167452	61.575749	34.701074	40.903407	40.903357	35.579722	80.180111
$\chi 2$	19.143894	12.139720	8.883432	5.153595	5.153595	9.880980	23.622059
HYBRID	76.575576	48.558880	35.533729	20.614381	20.614381	39.523920	94.488238
MPSD	2.157111	1.665528	0.405804	0.644455	0.644452	0.397610	2.417826
EABS	9.496719	9.784400	21.602410	13.620199	13.620226	22.939692	9.285896
SNE	4.954762	4.050463	4.006496	2.847339	**2.847338**	3.873087	5.516199

Table 8
Summarization of the determined error functions, sum of normalized errors (SNE), and parameter sets of the non-linear Toth isotherm model for AC-800.

	R^2	ERRSQ/SSE	ARE	χ2	HYBRID	MPSD	EABS
Temperature 0 °C							
q_m	18.5888	18.5880	15.0967	16.9315	16.9315	11.1395	17.7196
K_T	1.7320	1.7323	1.9677	1.8110	1.8110	2.4015	1.7724
n_T	0.4757	0.4757	0.5289	0.5005	0.5005	0.6304	0.4886
R^2	0.999981	0.999981	0.999905	0.999973	0.999973	0.999225	0.999976
ERRSQ	0.003117	0.003117	0.015719	0.004563	0.004563	0.126953	0.004077
ARE	2.351571	2.355321	1.765341	1.869985	1.869978	2.592740	1.965651
χ2	0.006640	0.006651	0.007131	0.005064	0.005064	0.037797	0.005635
HYBRID	0.014756	0.014781	0.015847	0.011253	0.011253	0.083993	0.012521
MPSD	0.064745	0.064786	0.048726	0.053900	0.053900	0.037436	0.059203
EABS	0.308533	0.308992	0.469294	0.326054	0.326051	1.468487	0.285302
SNE	3.492359	3.495347	3.253657	3.079135	**3.079134**	6.577080	3.196503
Temperature 25 °C							
q_m	23.2117	23.2046	21.1111	22.0880	22.0881	19.7322	23.5379
K_T	0.7092	0.7092	0.7573	0.7318	0.7318	0.7940	0.7036
n_T	0.4762	0.4763	0.4959	0.4870	0.4870	0.5108	0.4731
R^2	0.999999	0.999999	0.999994	0.999998	0.999998	0.999982	0.999999
ERRSQ	0.000052	0.000052	0.000341	0.000105	0.000105	0.000984	0.000057
ARE	0.244640	0.244345	0.241042	0.232454	0.232454	0.164357	0.257860
χ2	0.000200	0.000199	0.000188	0.000147	0.000147	0.000377	0.000244
HYBRID	0.000833	0.000827	0.000785	0.000614	0.000614	0.000838	0.001017
MPSD	0.007004	0.006974	0.004462	0.005157	0.005157	0.002717	0.007773
EABS	0.028531	0.028603	0.078427	0.046973	0.046972	0.128455	0.026142
SNE	4.574183	4.560236	5.391102	4.232127	**4.232123**	7.695828	5.018127

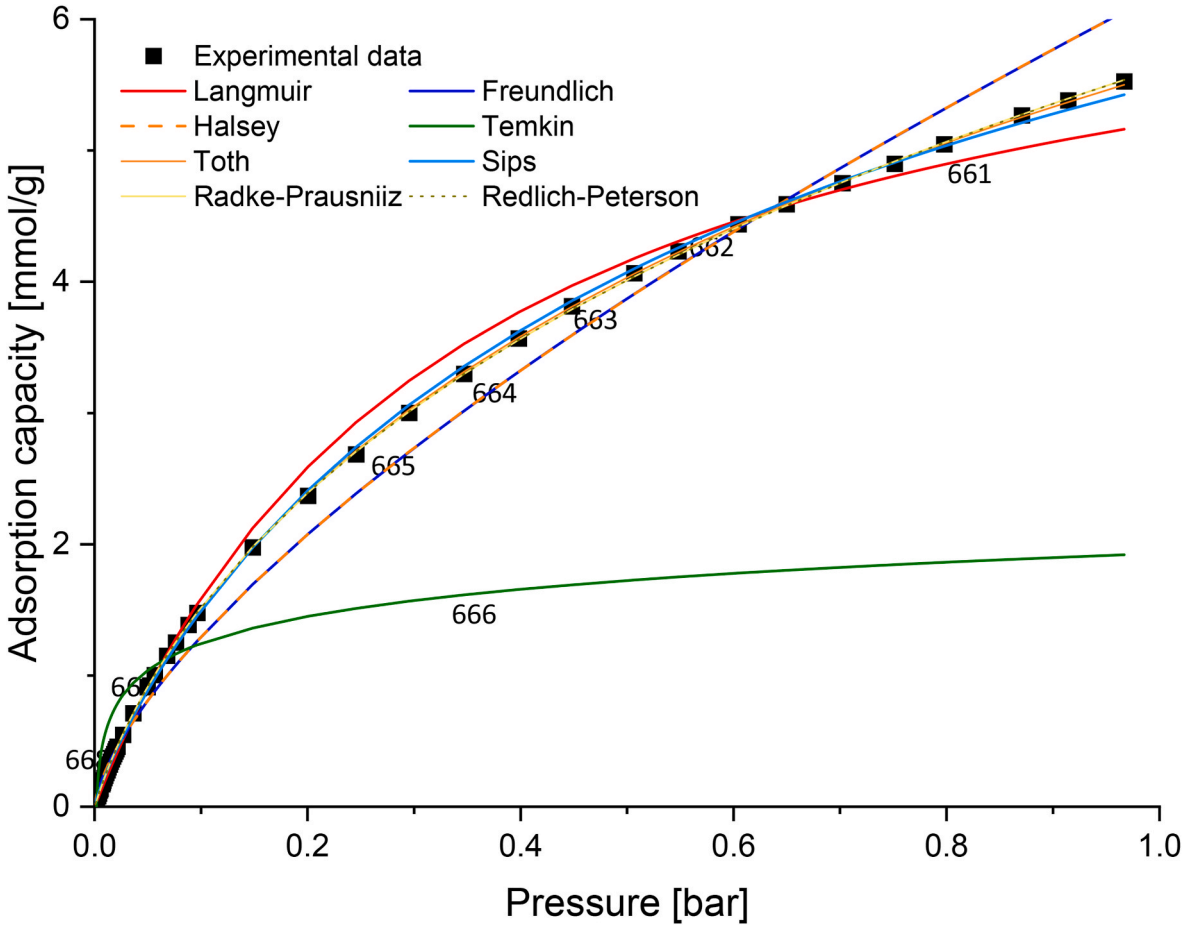

Fig. 7. CO_2 experimental equilibrium data at 0 °C with fitted non-linear isotherm models based on HYBRID error function for AC-800.

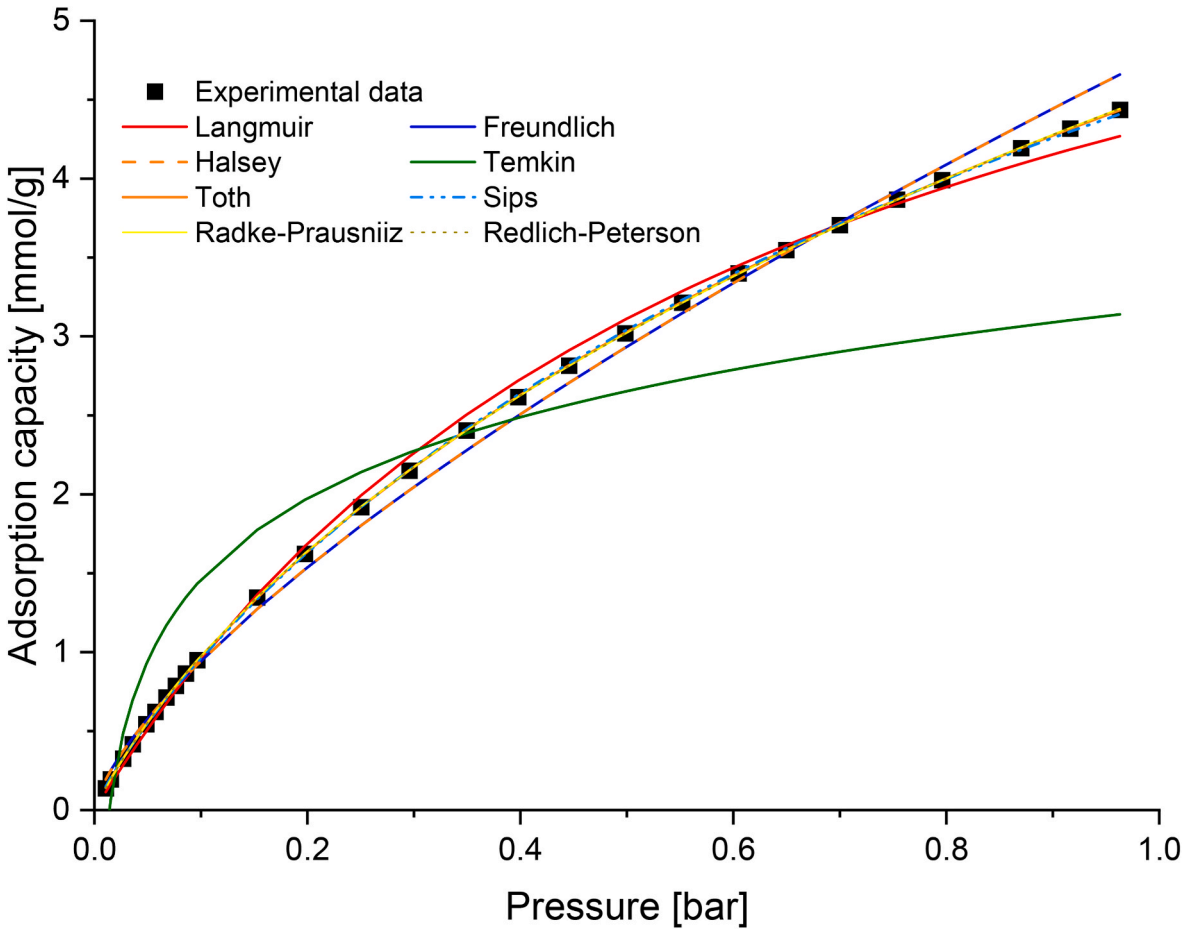

Fig. 8. CO_2 experimental equilibrium data at 25 °C with fitted non-linear isotherm models based on HYBRID error function for AC-800.

functions for the modelling of CO_2 adsorption equilibrium in AC. In sets of 64 adsorption systems (considering eight isotherms for four activated carbon samples at two adsorption temperatures), it was observed that the hybrid fractional error function (HYBRID), in conjunction with the chi-square test ($\chi 2$), yielded the principal overall performance. They make a clear distinction between isothermal models, for which the remaining statistical criteria offer equivocal results, and concepts that may rely on the number of measurement points, degrees of freedom of the adsorption system, and the relative pressure of CO_2. The specific reasons why the HYBRID and $\chi 2$ errors showed the lowest values of SNE in isotherm modeling series may vary depending on the specific details of the data and the model being applied. However, in general, HYBRID and $\chi 2$ errors are considered comprehensive tools in isotherm modeling because they are both robust and well-established measures of model accuracy that can help identify good-fitting models. The HYBRID error balances the influence of both large and small errors, while the $\chi 2$ error compares the deviation of the model's predicted values from the observed values, taking into account the uncertainty of the experimental values. Finally, it was determined that the HYBRID error function generated the most reliable data (in the case of the AC-800, the SNE varies between 1.9420 and 5.43661), providing the lowest SNE value for 41 systems, where $\chi 2$ was ranked as the second best for 19 different systems.

Based on this line of reasoning, HYBRID was chosen as the optimal error function for the purpose of ascertaining and analyzing the isotherm models that characterize the finest fit to the experimental data. Moreover, the SNE values for the chi square test differed insignificantly compared to HYBRID, equivalent to approximately 10^{-4} to 10^{-9}, which can suggest a similar effect on the predicted isotherm data regarding the analogous error structure. Among the rest of error functions, Marquardt's percent standard deviation (MPSD) was the most inappropriate one as a statical tool for non-linear mathematical modeling of CO_2 adsorption equilibrium on AC. The MPSD exhibited the largest discrepancies in the estimation of the rest errors, which had a direct negative impact on the SNE. In order to compare the fitting all eight evaluated isotherm models based on the HYBRID error function, their curve runs are illustrated in Figs. 7 and 8, for AC-800 at 0 and 25 °C.

As can be observed from Figs. 7 and 8, four three-parameter isotherm models are overlapping at some points and produce a forecast that is competitive in relation to the empirical data, including: Toth, Sips, Radke-Prausnitz, and Redlich-Peterson. Therefore, a careful analysis of the error functions obtained is recommended for each isotherm model. Table 4 displays the Langmuir isotherm constants and error functions that were calculated for AC-800. The HYBRID error function produced the optimal parameter in six out of the eight two-parameter models examined. Among the two-parameter isotherm models, the Langmuir model provided a better fit with high R^2 (0.995891–0.997594) and relatively low HYBRID (0.279697–0.644314) values than the

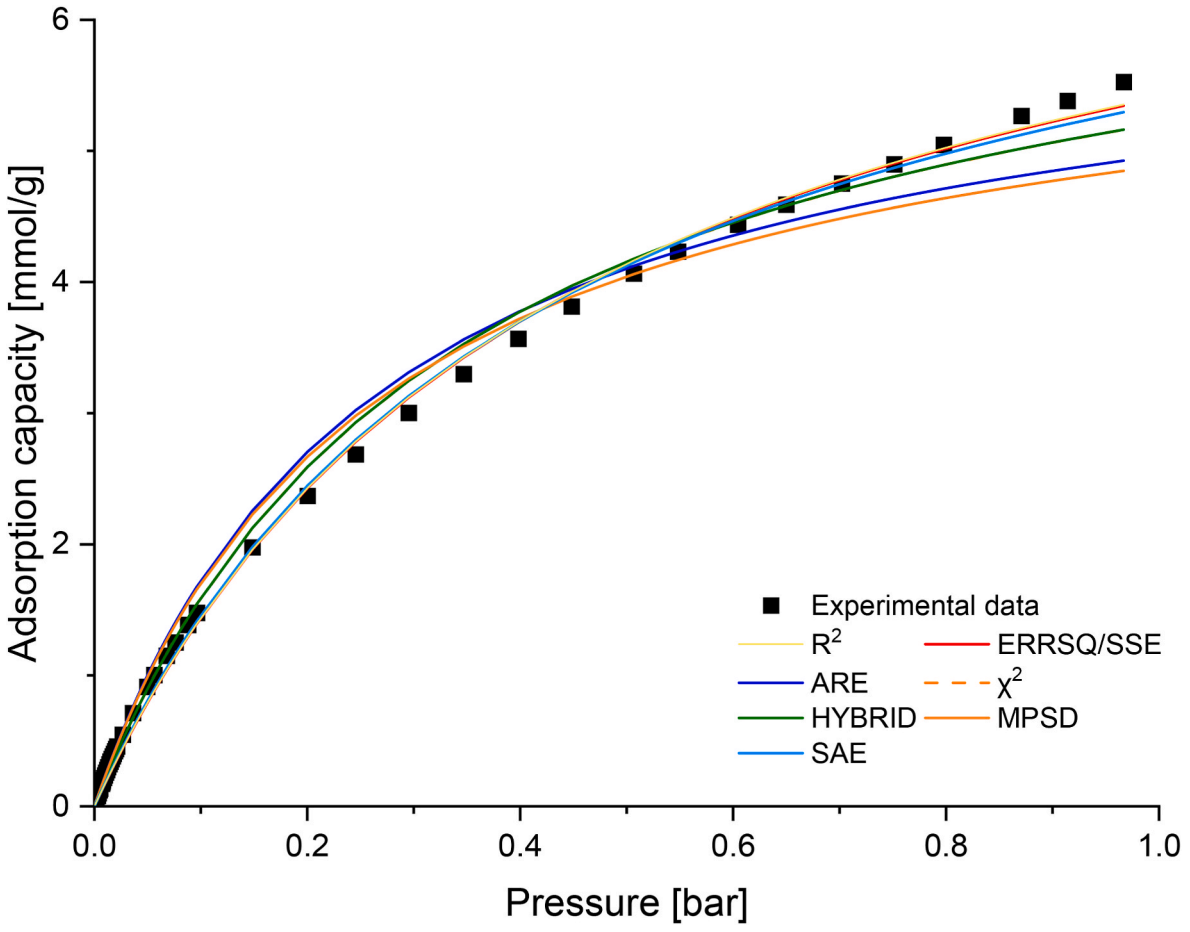

Fig. 9. Fitting the Langmuir isotherm curve to the experimental data based on different error functions for AC-800 at 0 °C.

Freundlich, Halsey (R^2: 0.991401–0.996113, HYBRID: 0.482912–1.592294) and Temkin (R^2: 0.273563–0.730479, HYBRID: 20.614381–73.756420) model in the studied relative pressure range. This demonstrates that the non-linear Langmuir isotherm model is superior to the other two-parameter isotherm models in regard to its capability to match the experimental data. When comparing the Langmuir model curve based on different error functions (Figs. 9 and 10), there is a noticeable difference between their courses throughout the entire examined pressure range. This confirms that each of the errors used generates a different value of the predicted model data, which may result in incorrect selection of the optimal one during modeling. Therefore, the use of the SNE procedure is such an important step that allows for the correct recognition of the CO_2 adsorption system on AC. With a detailed analysis of the SNE values, it is easy to determine the specific order of the function errors in relation to their degree of correlation with the equilibrium CO_2 data. In the case of the test CO_2-activated carbon (AC) complex for AC-800 at 0 °C, the calculated SNE is as follows for successive errors: R^2: 5.807925, ERRSQ/SSE: 5.773798, ARE: 5.551652, χ2: 4.343543, HYBRID: 4.343543, MPSD: 5.748482, and EABS: 5.444510. Following is a categorization of error functions that was made possible by the findings obtained by the SNE method, starting from the left with the error that best fits the model to the experimental data for AC-800:

χ2 > HYBRID > EABS > ARE > ERRSQ/SSE > MPS > R^2

while at 25 °C:

HYBRID > χ2 > ERRSQ/SSE > R^2 > EABS > ARE > MPS

For the two data series, there is a noticeable dominance by HYBRID and χ2 over the other errors when it comes to the smallest SNE values. During modeling, the initial values of the empirical isotherm points, which quantified the course of the isotherm curve, had the greatest impact on the error values obtained.

Tables 5 and 6 present the Freundlich and Halsey isotherm constants determined by non-linear regression and error functions. Taking into account the HYBRID values in Table 7 and the shape of the model curve, the Temkin isotherm was unable to characterize the equilibrium CO_2 adsorption data on activated carbon in a satisfactory manner, compared to Langmuir, Freundlich, and Halsey.

In terms of three-parameter isotherms, all models were characterized by extremely low hybrid fractional error function values, contrasted to models with only two parameters (in 6 of 8 sets, HYBRID was the preferable error function). Conclusions that may be drawn from the non-linear regression of the Toth isotherm (given in Table 8) exposed that the experimental findings were described exceptionally precisely (R^2: 0.999973–0.999998, HYBRID: 0.000614–0.005064), which may suggest CO_2 adsorption on the heterogeneous surface. For the remaining isothermal models, these values were varied, respectively, as fallows: Sips (R^2: 0.999934-0.999737, HYBRID: 0.012317–0.071389), Radke-

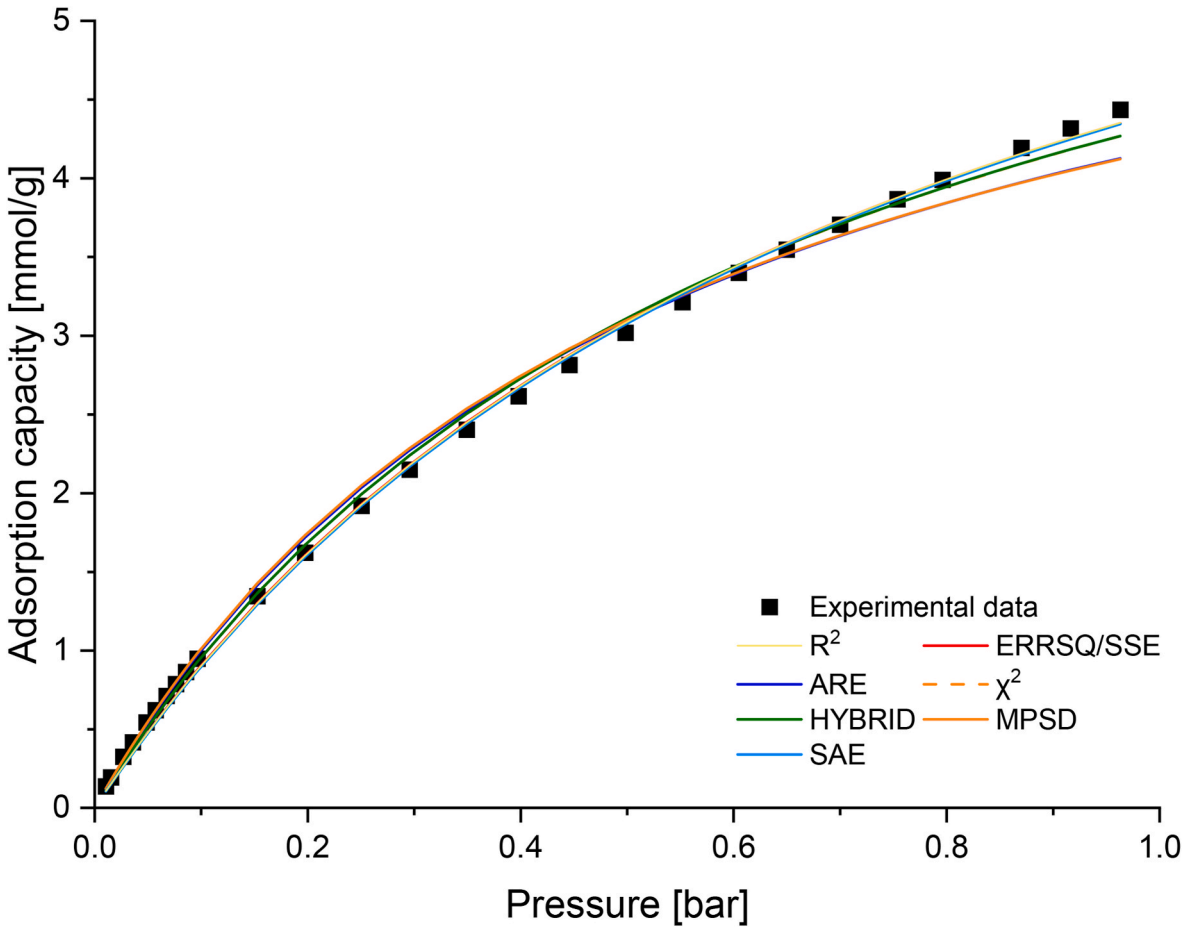

Fig. 10. Fitting the Langmuir isotherm curve to the experimental data based on different error functions for AC-800 at 25 °C.

Table 9
Summarization of the determined error functions, sum of normalized errors (SNE), and parameter sets of the non-linear Sips isotherm model for AC-800.

	R^2	ERRSQ/SSE	ARE	χ2	HYBRID	MPSD	EABS
Temperature 0 °C							
q_m	11.0271	11.0294	8.2242	9.6235	9.6235	7.1316	10.7465
K_S	1.0230	1.0223	1.9752	1.3940	1.3940	2.7287	1.0819
n_S	1.2255	1.2257	1.1164	1.1640	1.1640	1.0546	1.2095
R^2	0.999907	0.999907	0.998439	0.999737	0.999737	0.995350	0.999886
ERRSQ	0.015413	0.015412	0.254675	0.043888	0.043888	0.740819	0.018835
ARE	7.905490	7.927624	3.725715	4.544523	4.544523	4.589710	6.266616
χ2	0.068007	0.068350	0.072906	0.032125	0.032125	0.197429	0.049374
HYBRID	0.151127	0.151890	0.162014	0.071389	0.071389	0.438731	0.109721
MPSD	0.188999	0.189378	0.085617	0.114977	0.114977	0.057475	0.162409
EABS	0.770727	0.770201	1.942869	1.025619	1.025619	3.486595	0.679714
SNE	3.925990	3.934111	3.560165	2.859046	**2.859046**	5.877887	3.368598
Temperature 25 °C							
q_m	11.6973	11.8298	10.1543	10.7803	10.7808	9.3862	12.1583
K_S	0.5756	0.5629	0.7568	0.6773	0.6773	0.8848	0.5321
n_S	1.1861	1.1901	1.1480	1.1599	1.1599	1.1220	1.2003
R^2	0.999969	0.999970	0.999828	0.999934	0.999934	0.999620	0.999967
ERRSQ	0.001722	0.001672	0.009566	0.003689	0.003687	0.021147	0.001856
ARE	1.223074	1.281723	0.994768	1.020829	1.020855	0.629386	1.477625
χ2	0.004466	0.005034	0.003913	0.002956	0.002956	0.006970	0.006900
HYBRID	0.018607	0.020977	0.016303	0.012317	0.012317	0.015490	0.028751
MPSD	0.031471	0.033772	0.018365	0.020414	0.020417	0.009851	0.039599
EABS	0.179476	0.172821	0.374358	0.269036	0.268971	0.562276	0.163800
SNE	4.448022	4.705662	4.463428	3.800682	**3.800588**	5.256048	5.541605

Table 10
Summarization of the determined error functions, sum of normalized errors (SNE), and parameter sets of the non-linear Radke-Prausnitz isotherm model for AC-800.

	R^2	ERRSQ/SSE	ARE	χ2	HYBRID	MPSD	EABS
Temperature 0 °C							
q_m	7.0690	7.0685	7.0316	7.0489	7.0489	6.9923	7.0402
K_{RPr}	3.8693	3.8703	3.9780	3.9471	3.9471	3.7552	3.9317
e_{RPr}	0.6852	0.6852	0.6746	0.6774	0.6774	0.7319	0.6807
R^2	0.999973	0.999973	0.999966	0.999971	0.999971	0.999766	0.999969
ERRSQ	0.004549	0.004549	0.005672	0.004869	0.004869	0.038619	0.005129
ARE	1.550047	1.547215	1.395403	1.412119	1.412119	2.092602	1.421789
χ2	0.003731	0.003720	0.003434	0.003268	0.003268	0.015137	0.003401
HYBRID	0.008291	0.008266	0.007632	0.007262	0.007262	0.033637	0.007557
MPSD	0.036359	0.036383	0.040344	0.039236	0.039236	0.032953	0.038260
EABS	0.327988	0.327336	0.301767	0.318836	0.318836	0.904422	0.301383
SNE	3.615358	3.612372	3.601143	**3.557783**	3.557783	6.816592	3.543172
Temperature 25 °C							
q_m	6.5701	6.5666	6.5446	6.5437	6.5437	6.5393	6.5501
K_{RPr}	2.2288	2.2305	2.2703	2.2628	2.2628	2.2694	2.2603
e_{RPr}	0.6496	0.6493	0.6393	0.6429	0.6429	0.6413	0.6421
R^2	0.999997	0.999996	0.999993	0.999996	0.999996	0.999995	0.999995
ERRSQ	0.000189	0.000206	0.000372	0.000232	0.000232	0.000259	0.000282
ARE	0.203041	0.205387	0.120113	0.131577	0.131577	0.071494	0.127061
χ2	0.000131	0.000135	0.000109	0.000087	0.000087	0.000089	0.000096
HYBRID	0.000544	0.000563	0.000453	0.000361	0.000361	0.000197	0.000398
MPSD	0.003086	0.003114	0.001677	0.001652	0.001652	0.001173	0.001736
EABS	0.063670	0.065307	0.062828	0.062930	0.062930	0.064124	0.059623
SNE	6.397284	6.554889	5.693643	5.042492	**5.042492**	4.408526	5.261913

Table 11
Summarization of the determined error functions, sum of normalized errors (SNE), and parameter sets of the non-linear Redlich-Peterson isotherm model for AC-800.

	R^2	ERRSQ/SSE	ARE	χ2	HYBRID	MPSD	EABS
Temperature 0 °C							
q_m	27.3495	27.3567	27.9682	27.8226	27.8226	26.2570	27.8343
K_{RPr}	3.8689	3.8702	3.9780	3.9471	3.9471	3.7551	3.9559
B_{RP}	0.6852	0.6852	0.6747	0.6774	0.6774	0.7319	0.6773
R^2	0.999973	0.999973	0.999966	0.999971	0.999971	0.999766	0.999968
ERRSQ	0.004549	0.004549	0.005728	0.004869	0.004869	0.038615	0.005377
ARE	1.551436	1.547512	1.395547	1.412164	1.412164	2.092632	1.403563
χ2	0.003737	0.003721	0.003448	0.003268	0.003268	0.015137	0.003381
HYBRID	0.008304	0.008268	0.007663	0.007262	0.007262	0.033638	0.007514
MPSD	0.036348	0.036381	0.040320	0.039234	0.039234	0.032953	0.039321
EABS	0.328165	0.327374	0.302254	0.318841	0.318841	0.904361	0.301366
SNE	3.617237	3.613200	3.605063	**3.558326**	3.558326	6.817071	3.565166
Temperature 25 °C							
q_m	14.6413	14.6411	14.8576	14.8067	14.8067	14.8405	14.7780
K_{RPr}	2.2284	2.2283	2.2702	2.2627	2.2627	2.2694	2.2546
B_{RP}	0.6496	0.6496	0.6394	0.6429	0.6429	0.6413	0.6434
R^2	0.999997	0.999997	0.999993	0.999996	0.999996	0.999995	0.999995
ERRSQ	0.000189	0.000189	0.000369	0.000233	0.000232	0.000259	0.000269
ARE	0.204682	0.205053	0.120185	0.131507	0.131563	0.127076	0.133525
χ2	0.000132	0.000132	0.000108	0.000087	0.000087	0.000089	0.000098
HYBRID	0.000549	0.000550	0.000450	0.000361	0.000361	0.000369	0.000410
MPSD	0.003117	0.003125	0.001674	0.001655	0.001653	0.001607	0.001872
EABS	0.063771	0.063798	0.062676	0.062871	0.062906	0.064092	0.059524
SNE	7.034019	7.043568	6.049459	5.436782	**5.436615**	5.507954	5.745137

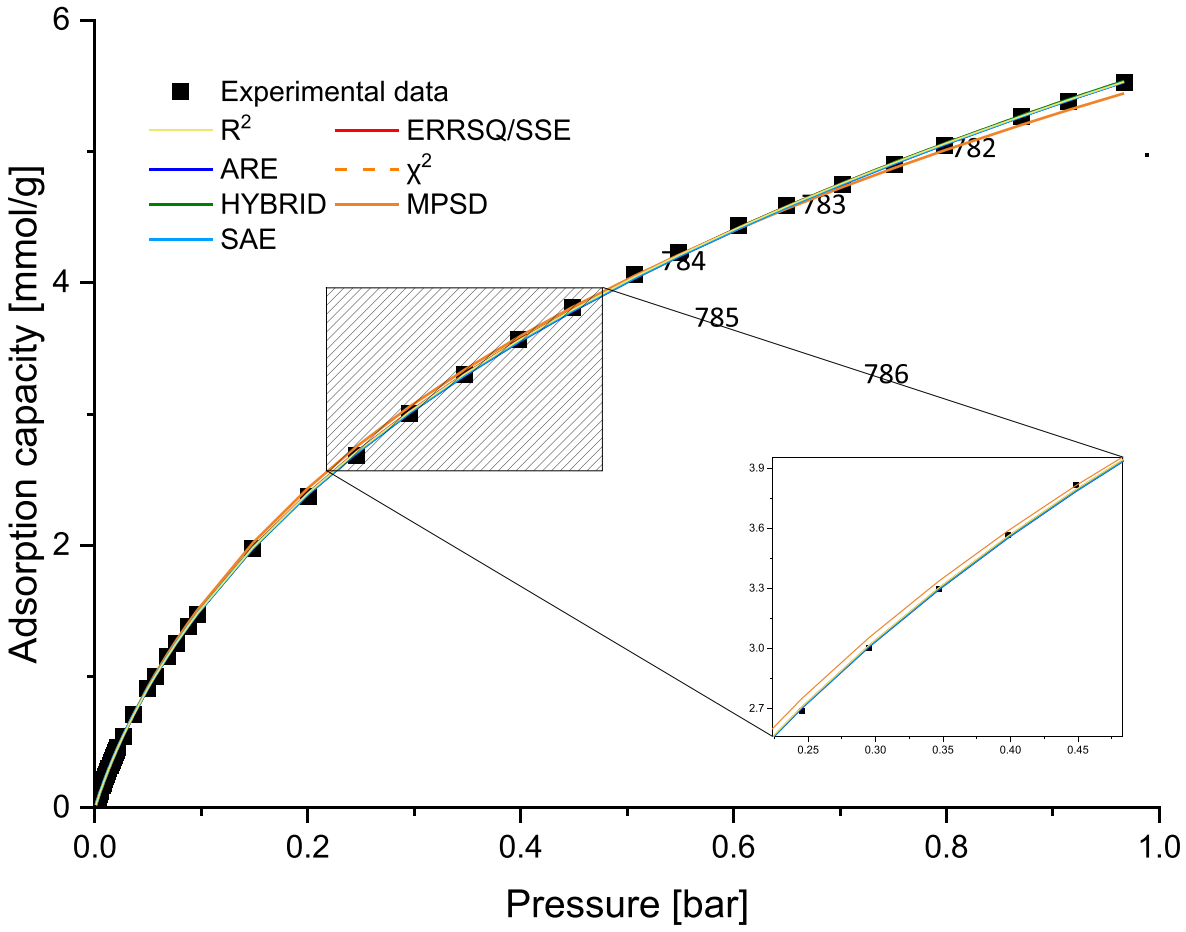

Fig. 11. Fitting the Radke-Prausnitz isotherm curve to the experimental data based on different error functions for AC-800 at 0 °C.

Prausnitz (R^2: 0.999971–0.999996, HYBRID: 0.000361–0.007262), and Redlich-Peterson (R^2: 0.999971–0.999996, HYBRID: 0.000361–0.007262). Their isotherms parameters and error analysis are included in Table 9, Table 10, and Table 11, respectively.

From the set of error functions in Tables 10 and 11, it can be clearly seen that their values for Radke-Prausnitz and Redlich-Peterson isotherm are completely identical, regarding the low concentration of the adsorbate in adsorption system. Moreover, they better correlate with CO_2 adsorption equilibrium data, due to the lower optimal error function. In accordance with the HYBRID, we ranked the degrees of fitting of the all isotherm models in the following order: (from the left isothermal model that possesses minimum error distribution to the experimental equilibrium for the studied AC-800 at 0 and 25 °C):

Redlich-Peterson = Radke-Prausnitz > Toth > Sips > Langmuir > Freundlich = Halsey > Temkin

The same sequence is also found for samples of AC-600, AC-700, and AC-900. Interpreting the above relationship made it possible to clearly define the choice of the Redlich-Peterson and Toth isotherm model as appropriate for the verification of research on the CO_2 adsorption system in AC (Radke-Prausnitz finds application only for a specific range of CO_2 concentration, without specifying the mechanism between the adsorbate-adsorbent complex). Because the β_{RP} value of Redlich-Peterson isotherm becomes closer to one (β_{RP}: 0.6747–0.7319 at 0 °C, β_{RP}: 0.6413–0.6496 at 25 °C), the model tends to be simplified down to the Langmuir model when applied to scenarios with low concentrations. On the contrary, all the heterogeneity factors of the Toth isotherm do not equal unity (n_T: 0.4757–0.6304 at 0 °C, n_T: 0.4731–0.5108 at 25 °C, which indicates the heterogeneity of the CO_2 - AC adsorption system. Moreover, the Toth model is an expression that rises steadily and monotonically, and it correctly depicts a great deal of systems with coverage submonolayer. Verification of selected assumptions of isothermal models leads to the conclusion that CO_2 storage in AC occurred in accordance with the submonolayer adsorption on the heterogenous surface of solid porous activated carbon (AC). Additionally, it is clear that the three-parameter model, compared to the two-parameter models, offered a better fit for the CO_2 adsorption equilibrium data. The course of the curves of the Redlich-Peterson, and Toth models based on different error functions, is given in Figs. 11 and 12 at 0 °C. An example of those two model fittings clearly emphasizes that without the SNE procedure, it would not be possible to select the correct model for the description of CO_2 adsorption on AC, selection of optimal isothermal parameters and error function. The implementation of SNE directly made it possible to recognize the mechanism of the adsorption process and to determine the nature of CO_2 binding in the specific pressure range.

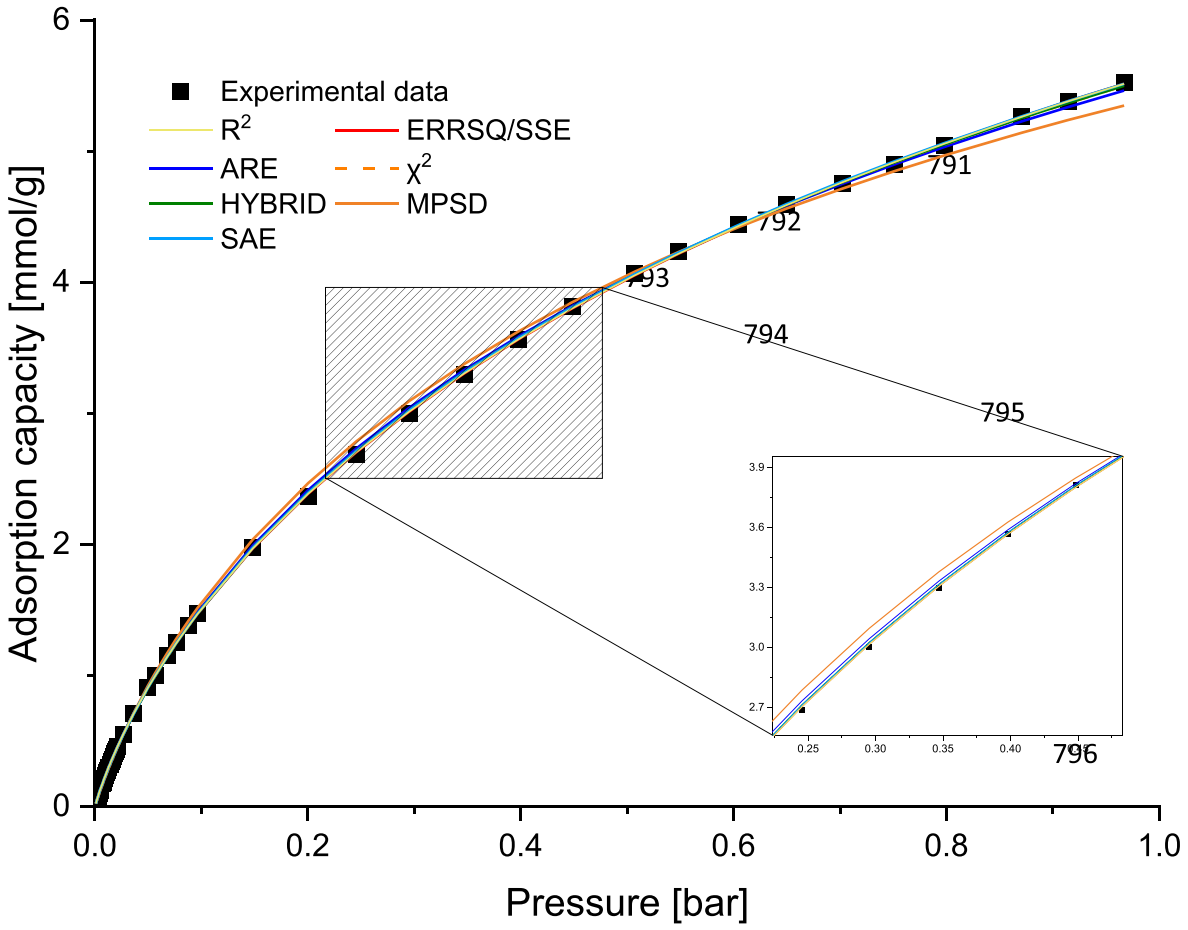

Fig. 12. Fitting the Toth isotherm curve to the experimental data based on different error functions for AC-800 at 0 °C.

4. Conclusions

This article emphasized the vital function of equilibrium adsorption isotherm modeling, along with material characterization, in the design and optimization of sorption systems in the sense of increasing the TRL. Consequently, we examined a detailed mathematical approach to the CO_2 adsorption process on activated carbon, using eight selected non-linear isothermal models and seven different error functions for this purpose. Based on the sum of normalized error (SNE), a comparison of the error functions was made, and the most accurate isotherm model, set of parameters, and error functions for correlation with the experimental data were identified. According to the statistical analysis, it was found that the three-parameter isotherms, Redlich-Peterson, Radke-Prausnitz, and Toth, best correlate with the experimental data in the entire pressure range for all AC samples. Due to the highest coefficient of determination (R^2) - close to one, with the lowest values of the determined error functions from the SNE procedure. The obtained results of fitting the nonlinearized form of isothermal models enabled the following graphic notation (from the left the best fitted model): Redlich-Peterson = Radke-Prausnitz > Toth > Sips > Langmuir > Freundlich = Halsey > Temkin. Interpretation of the values of individual SNE error functions also made it possible to select the most convenient and precise optimization criteria in the equilibrium sorption application. HYBRID and the chi-square test ($\chi 2$) were considered universal indicators in the prediction of isotherm modeling in sets of 64 adsorption systems, providing the best fit to the experimental data. The remaining statistical criteria gave a variety of outcomes, the nature of which may be contingent in part on the number of experimental points, model parameters, and pressure range. The entire sorption modeling methodology testified to the occurrence of the phenomenon of sub-monolayer adsorption on a heterogeneous surface. Finally, it was achieved to determine the nature of the CO_2 adsorption complex that is formed and to perform a detailed analysis of the mechanisms that prevail on the surface of activated carbon. The actual process of carbon dioxide adsorption was shown to be more accurately and realistically as a result of the selection of the model and error function that had the greatest match with the empirical data.

CRediT authorship contribution statement

Jarosław Serafin: Conceptualization, Data curation, Formal analysis, Investigation, Project administration, Supervision, Visualization, Writing – original draft, Writing – review & editing, Validation. **Bartosz Dziejarski:** Conceptualization, Data curation, Formal analysis, Investigation, Methodology, Software, Visualization, Writing – original draft, Writing – review & editing, Validation.

Declaration of competing interest

The authors declare that they have no known competing financial interests or personal relationships that could have appeared to influence the work reported in this paper.

Data availability

Data will be made available on request.

Acknowledgements

Jarosław Serafin is grateful to Spanish Ministry of Research and Innovation project no: PID2020-116031RBI00/AEI/10.13039/

501100011033/FEDER.

Appendix A. Supplementary data

Supplementary data to this article can be found online at https://doi.org/10.1016/j.micromeso.2023.112513.

References

[1] S.J. Davis, N.S. Lewis, M. Shaner, S. Aggarwal, D. Arent, I.L. Azevedo, K. Caldeira, Net-zero emissions energy systems, Science 360 (6396) (2018), https://doi.org/10.1126/science.aas9793.

[2] S.I. Zandalinas, F.B. Fritschi, R. Mittler, Global warming, climate change, and environmental pollution: recipe for a multifactorial stress combination disaster, Trends Plant Sci. 26 (6) (2021) 588–599, https://doi.org/10.1016/j.tplants.2021.02.011.

[3] R.P. Allan, E. Hawkins, N. Bellouin, B. Collins, IPCC, 2021: Summary for Policymakers, 2021, https://doi.org/10.1017/9781009157896.001.

[4] S. Impram, S.V. Nese, B. Oral, Challenges of renewable energy penetration on power system flexibility: a survey, Energy Strategy Rev. 31 (2020), 100539, https://doi.org/10.1016/j.esr.2020.100539.

[5] P.A. Çelik, D.Ö. Aksoy, S. Koca, H. Koca, A. Çabuk, The approach of biodesulfurization for clean coal technologies: a review, Int. J. Environ. Sci. Technol. 16 (4) (2019) 2115–2132, https://doi.org/10.1007/s13762-019-02232-7.

[6] J.F.D. Tapia, J.Y. Lee, R.E. Ooi, D.C. Foo, R.R. Tan, A review of optimization and decision-making models for the planning of CO2 capture, utilization and storage (CCUS) systems, Sustain. Prod. Consum. 13 (2018) 1–15, https://doi.org/10.1016/j.spc.2017.10.001.

[7] H. Zeng, X. Qu, D. Xu, Y. Luo, Porous adsorption materials for carbon dioxide capture in industrial flue gas, Front. Chem. 10 (2022), https://doi.org/10.3389/fchem.2022.939701.

[8] H. Marsh, F.R. Reinoso, Activated Carbon, Elsevier, 2006, https://doi.org/10.1016/B978-0-08-044463-5.X5013-4.

[9] K.V. Kumar, K. Porkodi, F. Rocha, Isotherms and thermodynamics by linear and non-linear regression analysis for the sorption of methylene blue onto activated carbon: comparison of various error functions, J. Hazard Mater. 151 (2–3) (2008) 794–804, https://doi.org/10.1016/j.jhazmat.2007.06.056.

[10] Langmuir, The adsorption of gases on plane surfaces of glass, mica and platinum, J. Am. Chem. Soc. 40 (1918) 1361–1403, https://doi.org/10.1021/ja02242a004.

[11] A. Dabrowski, Adsorption—from theory to practice, Adv. Colloid Interface Sci. 93 (2001) 135–224, https://doi.org/10.1016/S0001-8686(00)00082-8.

[12] H.M.F. Freundlich, Over the adsorption in solution, J. Phys. Chem. 57 (1906) 385–470.

[13] S. Basu, U.S. Shivhare, A.S. Mujumdar, Models for sorption isotherms for foods: a review, Dry. Technol. 24 (8) (2006) 917–930, https://doi.org/10.1080/07373930600775979.

[14] A.H. Al-Muhtaseb, W.A.M. McMinn, T.R.A. Magee, Moisture sorption isotherm characteristics of food products: a review, Food Bioprod. Process. 80 (2) (2002) 118–128, https://doi.org/10.1205/09603080252938753.

[15] N. Can, B.C. Ömür, A. Altındal, Modeling of heavy metal ion adsorption isotherms onto metallophthalocyanine film, Sensor. Actuator. B Chem. 237 (2016) 953–961, https://doi.org/10.1016/j.snb.2016.07.026.

[16] H.S. Ibrahim, T.S. Jamil, E.Z. Hegazy, Application of zeolite prepared from Egyptian kaolin for the removal of heavy metals: II. Isotherm models, J. Hazard Mater. 182 (1–3) (2010) 842–847, https://doi.org/10.1016/j.jhazmat.2010.06.118.

[17] M. Hadi, M.R. Samarghandi, G. McKay, Equilibrium two-parameter isotherms of acid dyes sorption by activated carbons: study of residual errors, Chem. Eng. J. 160 (2) (2010) 408–416, https://doi.org/10.1016/j.cej.2010.03.016.

[18] M.Ş. Tanyildizi, Modeling of adsorption isotherms and kinetics of reactive dye from aqueous solution by peanut hull, Chem. Eng. J. 168 (3) (2011) 1234–1240, https://doi.org/10.1016/j.cej.2011.02.021.

[19] J. Li, C.J. Werth, Modeling sorption isotherms of volatile organic chemical mixtures in model and natural solids, Environ. Toxicol. Chem.: Int. J. 21 (7) (2002) 1377–1383, https://doi.org/10.1002/etc.5620210707.

[20] D.T. Tefera, Z. Hashisho, J.H. Philips, J.E. Anderson, M. Nichols, Modeling competitive adsorption of mixtures of volatile organic compounds in a fixed-bed of beaded activated carbon, Eviron. Sci. Technol. 48 (9) (2014) 5108–5117, https://doi.org/10.1021/es404667f.

[21] J. Serafin, M. Ouzzine, C. Xing, H. El Ouahabi, A. Kamińska, J. Sreńscek-Nazzal, Activated carbons from the Amazonian biomass andiroba shells applied as a CO2 adsorbent and a cheap semiconductor material, J. CO2 Util. 62 (2022), 102071, https://doi.org/10.1016/j.jcou.2022.102071.

[22] J. Serafin, B. Dziejarski, O.F.C. Junior, J. Sreńscek-Nazzal, Design of highly microporous activated carbons based on walnut shell biomass for H2 and CO2 storage, Carbon 201 (2023) 633–647, https://doi.org/10.1016/j.carbon.2022.09.013.

[23] G.G. Huang, Y.F. Liu, X.X. Wu, J.J. Cai, Activated carbons prepared by the KOH activation of a hydrochar from garlic peel and their CO2 adsorption performance, N. Carbon Mater. 34 (3) (2019) 247–257, https://doi.org/10.1016/S1872-5805(19)60014-4.

[24] Jarosław Serafin, Joanna Sreńscek-Nazzal, Adrianna Kamińska, Oliwia Paszkiewicz, Beata Michalkiewicz, Management of surgical mask waste to activated carbons for CO2 capture, J. CO2 Util. 59 (2022), 101970, https://doi.org/10.1016/j.jcou.2022.101970.

[25] A. Arenillas, K.M. Smith, T.C. Drage, C.E. Snape, CO2 capture using some fly ash-derived carbon materials, Fuel 84 (17) (2005) 2204–2210, https://doi.org/10.1016/j.fuel.2005.04.003.

[26] F.O. Ochedi, Y. Liu, Y.G. Adewuyi, State-of-the-art review on capture of CO2 using adsorbents prepared from waste materials, Process Saf. Environ. Protect. 139 (2020) 1–25, https://doi.org/10.1016/j.psep.2020.03.036.

[27] F. Raganati, F. Miccio, P. Ammendola, Adsorption of carbon dioxide for post-combustion capture: a review, Energy Fuel. 35 (16) (2021) 12845–12868, https://doi.org/10.1021/acs.energyfuels.1c01618.

[28] J. Zhang, P.A. Webley, P. Xiao, Effect of process parameters on power requirements of vacuum swing adsorption technology for CO2 capture from flue gas, Energy Convers. Manag. 49 (2) (2008) 346–356, https://doi.org/10.1016/j.enconman.2007.06.007.

[29] K. Wang, H. Shang, L. Li, X. Yan, Z. Yan, C. Liu, Q. Zha, Efficient CO2 capture on low-cost silica gel modified by polyethyleneimine, J. Nat. Gas Chem. 21 (3) (2012) 319–323, https://doi.org/10.1016/S1003-9953(11)60371-X.

[30] E.S. Kikkinides, R.T. Yang, S.H. Cho, Concentration and recovery of carbon dioxide from flue gas by pressure swing adsorption, Ind. Eng. Chem. Res. 32 (11) (1993) 2714–2720, https://doi.org/10.1021/ie00023a038.

[31] D. Aaron, C. Tsouris, Separation of CO2 from flue gas: a review, Separ. Sci. Technol. 40 (1–3) (2005) 321–348, https://doi.org/10.1081/SS-200042244.

[32] J.C. Groen, L.A. Peffer, J. Pérez-Ramírez, Pore size determination in modified micro-and mesoporous materials. Pitfalls and limitations in gas adsorption data analysis, Microporous Mesoporous Mater. 60 (1–3) (2003) 1–17, https://doi.org/10.1016/S1387-1811(03)00339-1.

[33] C. Tien, Introduction to Adsorption: Basics, Analysis, and Applications, Elsevier, 2018, https://doi.org/10.1016/C2018-0-00297-2. Introduction to Adsorption: Basics, Analysis, and Applications, Chi Tien, 2018.

[34] J. Rouquerol, F. Rouquerol, P. Llewellyn, G. Maurin, K.S. Sing, Adsorption by Powders and Porous Solids: Principles, Methodology and Applications, Academic press, 2013, https://doi.org/10.1016/B978-0-12-598920-6.X5000-3.

[35] M. Ghaedi (Ed.), Adsorption: Fundamental Processes and Applications, Academic Press, 2021.

[36] D. Danaci, P.A. Webley, C. Petit, Guidelines for techno-economic analysis of adsorption processes, Front. Chem. Eng. 30 (2021), https://doi.org/10.3389/fceng.2020.602430.

[37] C. Erkey, Thermodynamics and dynamics of adsorption of metal complexes on surfaces from supercritical solutions, in: Supercritical Fluid Science and Technology, vol. 1, Elsevier, 2011, pp. 41–77, https://doi.org/10.1016/B978-0-08-045329-3.00004-4.

[38] J.C. Pashin, Coal as a petroleum source rock and reservoir rock, in: Applied Coal Petrology, Elsevier, 2008, pp. 227–262, https://doi.org/10.1016/B978-0-08-045051-3.00009-9.

[39] D.A. Bell, B.F. Towler, M. Fan, Coal Gasification and its Applications, William Andrew, 2010, https://doi.org/10.1016/C2009-0-20067-5.

[40] I. Sarbu, C. Sebarchievici, Solar Heating and Cooling Systems: Fundamentals, Experiments and Applications, Academic Press, 2016.

[41] P.A. Webb, Introduction to Chemical Adsorption Analytical Techniques and Their Applications to Catalysis, Micromeritics Instrument Corp. Technical Publications, 2003, pp. 1–12.

[42] K.D. Hammond, W.C. Conner Jr., Analysis of catalyst surface structure by physical sorption, in: Advances in Catalysis, vol. 56, Academic Press, 2013, pp. 1–101, https://doi.org/10.1016/B978-0-12-420173-6.00001-2.

[43] N. Jaffrezic-Renault, H. Poirier-Andrade, D.H. Trang, Models for the adsorption of uranium on titanium dioxide, J. Chromatogr. A 201 (1980) 187–192, https://doi.org/10.1016/S0021-9673(00)83873-X.

[44] E. Worch, Adsorption technology in water treatment, in: Adsorption Technology in Water Treatment, de Gruyter, 2021, https://doi.org/10.1515/9783110240238.

[45] R.L. Burwell Jr., Manual of symbols and terminology for physicochemical quantities and units—appendix II heterogeneous catalysis, in: Advances in Catalysis, vol. 26, Academic Press, 1977, pp. 351–392, https://doi.org/10.1016/S0360-0564(08)60074-7.

[46] J.G. Carriazo, M. Moreno-Forero, R.A. Molina, S. Moreno, Incorporation of titanium and titanium–iron species inside a smectite-type mineral for photocatalysis, Appl. Clay Sci. 50 (3) (2010) 401–408, https://doi.org/10.1016/j.clay.2010.09.007.

[47] G. Wypych, Handbook of adhesion promoters. https://doi.org/10.1016/B978-1-927885-29-1.50004-3, 2018.

[48] V. Bolis, Fundamentals in adsorption at the solid-gas interface. Concepts and thermodynamics, in: Calorimetry and Thermal Methods in Catalysis, Springer, Berlin, Heidelberg, 2013, pp. 3–50, https://doi.org/10.1007/978-3-642-11954-5_1.

[49] M.J. Phele, I.P. Ejidike, F.M. Mtunzi, Adsorption efficiency of activated macadamia nutshell for the removal Organochlorine pesticides: endrin and 4, 4-DDT from aqueous solution, J. Pharmaceut. Sci. Res. 11 (1) (2019) 258–262.

[50] S. Raghav, D. Kumar, Adsorption equilibrium, kinetics, and thermodynamic studies of fluoride adsorbed by tetrametallic oxide adsorbent, J. Chem. Eng. Data 63 (5) (2018) 1682–1697, https://doi.org/10.1021/acs.jced.8b00024.

[51] S.U. Rege, R.T. Yang, A simple parameter for selecting an adsorbent for gas separation by pressure swing adsorption, Separ. Sci. Technol. 36 (15) (2001) 3355–3365, https://doi.org/10.1081/SS-100107907.

[52] J. Helminen, J. Helenius, E. Paatero, I. Turunen, Comparison of sorbents and isotherm models for NH3-gas separation by adsorption, AIChE J. 46 (8) (2000) 1541–1555, https://doi.org/10.1002/aic.690460807.

[53] Y. Sun, G. Yang, J.P. Zhang, Y. Wang, M.S. Yao, Activated carbon preparation from lignin by H3PO4 activation and its application to gas separation, Chem. Eng. Technol. 35 (2) (2012) 309–316, https://doi.org/10.1002/ceat.201100309.
[54] J.R. Li, R.J. Kuppler, H.C. Zhou, Selective gas adsorption and separation in metal–organic frameworks, Chem. Soc. Rev. 38 (5) (2009) 1477–1504, https://doi.org/10.1039/B802426J.
[55] Y.S. Ho, Selection of optimum sorption isotherm, Carbon 42 (10) (2004) 2115–2116, https://doi.org/10.1016/j.carbon.2004.03.019.
[56] K.V. Kumar, Optimum sorption isotherm by linear and non-linear methods for malachite green onto lemon peel, Dyes Pigments 74 (3) (2007) 595–597, https://doi.org/10.1016/j.dyepig.2006.03.026.
[57] Y.S. Ho, Isotherms for the sorption of lead onto peat: comparison of linear and non-linear methods, Pol. J. Environ. Stud. 15 (1) (2006).
[58] Y.C. Wong, Y.S. Szeto, W. Cheung, G. McKay, Adsorption of acid dyes on chitosan—equilibrium isotherm analyses, Process Biochem. 39 (6) (2004) 695–704, https://doi.org/10.1016/S0032-9592(03)00152-3.
[59] Y.S. Ho, W.T. Chiu, C.C. Wang, Regression analysis for the sorption isotherms of basic dyes on sugarcane dust, Bioresour. Technol. 96 (11) (2005) 1285–1291, https://doi.org/10.1016/j.biortech.2004.10.021.
[60] K.V. Kumar, Comparative analysis of linear and non-linear method of estimating the sorption isotherm parameters for malachite green onto activated carbon, J. Hazard Mater. 136 (2) (2006) 197–202, https://doi.org/10.1016/j.jhazmat.2005.09.018.
[61] K.V. Kumar, S. Sivanesan, Pseudo second order kinetics and pseudo isotherms for malachite green onto activated carbon: comparison of linear and non-linear regression methods, J. Hazard Mater. 136 (3) (2006) 721–726, https://doi.org/10.1016/j.jhazmat.2006.01.003.
[62] I. Langmuir, The constitution and fundamental properties of solids and liquids. Part I. Solids, J. Am. Chem. Soc. 38 (11) (1916) 2221–2295, https://doi.org/10.1021/ja02268a002.
[63] I. Langmuir, The adsorption of gases on plane surfaces of glass, mica and platinum, J. Am. Chem. Soc. 40 (9) (1918) 1361–1403, https://doi.org/10.1021/ja02242a004.
[64] K. Vijayaraghavan, T.V.N. Padmesh, K. Palanivelu, M. Velan, Biosorption of nickel (II) ions onto Sargassum wightii: application of two-parameter and three parameter isotherm models, J. Hazard Mater. B133 (2006) 304–308, https://doi.org/10.1016/j.jhazmat.2005.10.016.
[65] S. Kundu, A.K. Gupta, Arsenic adsorption onto iron oxide-coated cement (IOCC): regression analysis of equilibrium data with several isotherm models and their optimization, Chem. Eng. J. 122 (1–2) (2006) 93–106, https://doi.org/10.1016/j.cej.2006.06.002.
[66] H.M.F. Freundlich, Over the adsorption in solution, J. Phys. Chem. 57 (385471) (1906) 1100–1107.
[67] J. Zeldowitsch, Adsorption site energy distribution, Acta Phys. Chim. URSS 1 (1) (1934) 961–973.
[68] F. Haghseresht, G.Q. Lu, Adsorption characteristics of phenolic compounds onto coal-reject-derived adsorbents, Energy Fuel. 12 (6) (1998) 1100–1107, https://doi.org/10.1021/ef9801165.
[69] M.I. Temkin, Kinetics of ammonia synthesis on promoted iron catalysts, Acta Physiochim. URSS 12 (1940) 327–356.
[70] C. Aharoni, M. Ungarish, Kinetics of activated chemisorption. Part 2.—theoretical models, J. Chem. Soc., Faraday Trans. 1: Physical Chemistry in Condensed Phases 73 (1977) 456–464, https://doi.org/10.1039/F19777300456.
[71] Y. Kim, C. Kim, I. Choi, S. Rengaraj, J. Yi, Arsenic removal using mesoporous alumina prepared via a templating method, Eviron. Sci. Technol. 38 (3) (2004) 924–931, https://doi.org/10.1021/es0346431.
[72] G. Halsey, Physical adsorption on non-uniform surfaces, J. Chem. Phys. 16 (10) (1948) 931–937, https://doi.org/10.1063/1.1746689.
[73] J. Toth, State equation of the solid-gas interface layers, Acta Chim. Hung. 69 (1971) 311–328.
[74] J. Tóth, Calculation of the BET-compatible surface area from any type I isotherms measured above the critical temperature, J. Colloid Interface Sci. 225 (2) (2000) 378–383, https://doi.org/10.1006/jcis.2000.6723.
[75] J. Tóth, Uniform interpretation of gas/solid adsorption, Adv. Colloid Interface Sci. 55 (1995) 1–239, https://doi.org/10.1016/0001-8686(94)00226-3.
[76] M.V. Subbaiah, D.S. Kim, Adsorption of methyl orange from aqueous solution by aminated pumpkin seed powder: kinetics, isotherms, and thermodynamic studies, Ecotoxicol. Environ. Saf. 128 (2016) 109–117, https://doi.org/10.1016/j.ecoenv.2016.02.016.
[77] R. Sips, On the structure of a catalyst surface, J. Chem. Phys. 16 (5) (1948) 490–495, https://doi.org/10.1063/1.1746922.
[78] A. Günay, E. Arslankaya, I. Tosun, Lead removal from aqueous solution by natural and pretreated clinoptilolite: adsorption equilibrium and kinetics, J. Hazard Mater. 146 (1–2) (2007) 362–371, https://doi.org/10.1016/j.jhazmat.2006.12.034.
[79] A.B. Pérez-Marín, V.M. Zapata, J.F. Ortuno, M. Aguilar, J. Sáez, M. Lloréns, Removal of cadmium from aqueous solutions by adsorption onto orange waste, J. Hazard Mater. 139 (1) (2007) 122–131, https://doi.org/10.1016/j.jhazmat.2006.06.008.
[80] O.J.D.L. Redlich, D.L. Peterson, A useful adsorption isotherm, J. Phys. Chem. 63 (6) (1959), https://doi.org/10.1021/j150576a611, 1024-1024.
[81] R.K. Prasad, S.N. Srivastava, Sorption of distillery spent wash onto fly ash: kinetics and mass transfer studies, Chem. Eng. J. 146 (1) (2009) 90–97, https://doi.org/10.1016/j.cej.2008.05.021.
[82] F. Gimbert, N. Morin-Crini, F. Renault, P.M. Badot, G. Crini, Adsorption isotherm models for dye removal by cationized starch-based material in a single component system: error analysis, J. Hazard Mater. 157 (1) (2008) 34–46, https://doi.org/10.1016/j.jhazmat.2007.12.072.
[83] L. Jossens, J.M. Prausnitz, W. Fritz, E.U. Schlünder, A.L. Myers, Thermodynamics of multi-solute adsorption from dilute aqueous solutions, Chem. Eng. Sci. 33 (8) (1978) 1097–1106, https://doi.org/10.1016/0009-2509(78)85015-5.
[84] C.J. Radke, J.M. Prausnitz, Adsorption of organic solutes from dilute aqueous solution of activated carbon, Ind. Eng. Chem. Fundam. 11 (4) (1972) 445–451, https://doi.org/10.1021/i160044a003.
[85] Y.S. Ho, J.F. Porter, G. McKay, Equilibrium isotherm studies for the sorption of divalent metal ions onto peat: copper, nickel and lead single component systems, Water Air Soil Pollut. 141 (1) (2002) 1–33, https://doi.org/10.1023/A:1021304828010.
[86] K.Y. Foo, B.H. Hameed, Insights into the modeling of adsorption isotherm systems, Chem. Eng. J. 156 (1) (2010) 2–10, https://doi.org/10.1016/j.cej.2009.09.013.
[87] N. Sivarajasekar, R. Baskar, Adsorption of Basic Magenta II onto H2SO4 activated immature Gossypium hirsutum seeds: kinetics, isotherms, mass transfer, thermodynamics and process design, Arab. J. Chem. 12 (7) (2019) 1322–1337, https://doi.org/10.1016/j.arabjc.2014.10.040.
[88] T.M. Elmorsi, Equilibrium isotherms and kinetic studies of removal of methylene blue dye by adsorption onto miswak leaves as a natural adsorbent, J. Environ. Protect. 2 (2011) 817, https://doi.org/10.4236/jep.2011.26093, 06.
[89] D. Karadag, Y. Koc, M. Turan, M. Ozturk, A comparative study of linear and non-linear regression analysis for ammonium exchange by clinoptilolite zeolite, J. Hazard Mater. 144 (1–2) (2007) 432–437, https://doi.org/10.1016/j.jhazmat.2006.10.055.
[90] B. Boulinguiez, P. Le Cloirec, D. Wolbert, Revisiting the determination of Langmuir Parameters application to tetrahydrothiophene adsorption onto activated carbon, Langmuir 24 (13) (2008) 6420–6424, https://doi.org/10.1021/la800725s.
[91] J.C.Y. Ng, W.H. Cheung, G. McKay, Equilibrium studies for the sorption of lead from effluents using chitosan, Chemosphere 52 (6) (2003) 1021–1030, https://doi.org/10.1016/S0045-6535(03)00223-6.
[92] J.F. Porter, G. McKay, K.H. Choy, The prediction of sorption from a binary mixture of acidic dyes using single-and mixed-isotherm variants of the ideal adsorbed solute theory, Chem. Eng. Sci. 54 (24) (1999) 5863–5885, https://doi.org/10.1016/S0009-2509(99)00178-5.
[93] J.C.Y. Ng, W.H. Cheung, G. McKay, Equilibrium studies of the sorption of Cu (II) ions onto chitosan, J. Colloid Interface Sci. 255 (1) (2002) 64–74, https://doi.org/10.1006/jcis.2002.8664.
[94] A. Seidel, D. Gelbin, On applying the ideal adsorbed solution theory to multicomponent adsorption equilibria of dissolved organic components on activated carbon, Chem. Eng. Sci. 43 (1) (1988) 79–88, https://doi.org/10.1016/0009-2509(88)87128-8.
[95] D.W. Marquardt, An algorithm for least-squares estimation of nonlinear parameters, J. Soc. Ind. Appl. Math. 11 (2) (1963) 431–441, https://doi.org/10.1137/0111030.
[96] A.R. Khan, T.A. Al-Bahri, A. Al-Haddad, Adsorption of phenol based organic pollutants on activated carbon from multi-component dilute aqueous solutions, Water Res. 31 (8) (1997) 2102–2112, https://doi.org/10.1016/S0043-1354(97)00043-2.
[97] A. Kapoor, R.T. Yang, Correlation of equilibrium adsorption data of condensible vapours on porous adsorbents, Gas Separ. Purif. 3 (4) (1989) 187–192, https://doi.org/10.1016/0950-4214(89)80004-0.
[98] M. Ouzzine, J. Serafin, J. Sreńscek-Nazzal, Single step preparation of activated biocarbons derived from pomegranate peels and their CO2 adsorption performance, J. Anal. Appl. Pyrol. 160 (2021), 105338, https://doi.org/10.1016/j.jaap.2021.105338.